Wavelet Based Denoising of ECG Signals

A dissertation
submitted in partial fulfillment of
the requirements for the degree of

Master of Technology

by

T. Pranava
(10330010)

Under the supervision of

Prof. P. C. Pandey

Biomedical Engineering Group
Department of Biosciences and Bioengineering
Indian Institute of Technology Bombay
June 2012

This page is intentionally left blank

Indian Institute of Technology, Bombay

M. Tech. Dissertation Approval

This dissertation entitled **"Wavelet Based Denoising of ECG Signals"** by **T. Pranava** (Roll No. **10330010**) is approved, after the successful completion of *viva voce* examination, for the award of the degree of **Master of Technology** in **Biomedical Engineering.**

Supervisor .... 20/6/2012 (Prof. P. C. Pandey)

Examiners .... (Prof. V. K. Madan)

.... (Prof. V. M. Gadre)

Chairperson .... 20/6/12 (Prof. K. Chatterjee)

Date: 20 June, 2012

Place: Mumbai

This page is intentionally left blank

Declaration

I declare that this written submission represents my ideas and my own words and where other's ideas have been included, I have adequately cited and referenced the original sources. I also declare that I have adhered to all principles of academic honesty and integrity and have not misrepresented or fabricated or falsified any idea/data/fact/source in my submission. I understand that any violation of above will cause for disciplinary action by the institute and can also evoke penal action from the sources which have thus not been properly cited or from whom proper permission has not been taken when needed.

Pranava.T

Date: 1 June, 2012 Pranava T.

Place: Mumbai (10330010)

T. Pranava / Prof. P. C. Pandey (Supervisor), "Wavelet Based Denoising of ECG Signals", *M.Tech. Dissertation*, Biomedical Engineering Group, Department of Biosciences and Bioengineering, Indian Institute of Technology Bombay, June 2012.

ABSTRACT

Electrocardiography is an important non-invasive diagnostic tool for identifying cardiac disorders. It is usually prone to noise and artifacts. Wavelet based denoising techniques, using discrete Meyer wavelet function, were investigated for EMG and motion artifact suppression in ECG, and the use of translation-invariant wavelet denoising and stationary wavelet transform based denoising were investigated for suppressing the effect of Gibbs phenomenon introduced by discrete wavelet transform based denoising. EMG noise is suppressed using level-dependent thresholding and motion artifact is suppressed using coefficient clipping technique. The technique resulted in efficient denoising with no significant distortions introduced. SNR improvement, percentage RMS difference, L2 norm and MaxMin based improvement indices, and R-peak detection efficiency were used for quantitative evaluation. Artifact-free ECG signals from MIT-BIH arrhythmia database and ECG-free artifacts from MIT-BIH noise stress test database were used to generate simulated noisy signals with known SNR. For an input SNR of -10 dB, the SNR improvement of 14.5, 15.0 and 14.7 dB were obtained for DWT, TIWT and SWT based denoising, respectively. A correlation coefficient value of 0.99 was observed between denoised ECG and artifact-free ECG signals, indicating insignificant distortion of noise-free signals. An improvement in QRS detection efficiency from 94.4 % to 99.3 % with reduction in false detection percentage from 21.2 % to 14.9 % was obtained. The denoising techniques were also validated for ambulatory ECG signals from normal subjects and patients with cardiac abnormality available at MIT-BIH ECG databases and sudden cardiac death database. Significant improvement in QRS detection efficiency from 63.2 % to 90.6 % with reduction in false detection percentage from 0.1 % to 0.05 % was obtained. A software application "ECG Denoiser, v.2" has been developed incorporating DWT based ECG denoising for artifact suppression in 3-lead ECG signals acquired from Holter monitor with a sampling frequency of 200 Hz using LabWindows.

CONTENTS

List of Figures

List of Tables

List of Abbreviations

DWT	discrete wavelet transform
ECG	Electrocardiogram
EMG	Electromyogram
EMD	empirical mode decomposition
ICA	independent component analysis
II	improvement index
LMS	least mean squares
MSE	mean square error
PRD	percentage root mean square difference
RMSE	root mean square error
SER	signal-to-error ratio
SNR	signal-to-noise ratio
SWT	stationary wavelet transform
SURE	Stein's unbiased risk estimate
TIWT	translation-invariant wavelet transform
WEDD	wavelet energy-based diagnostic distortion
WWPRD	wavelet weighted percentage root mean square difference

This page is intentionally left blank

List of Symbols

$D(n)$	unmodified wavelet coefficients
$\hat{D}(n)$	modified wavelet coefficients
$e(n)$	error signal
r	correlation coefficient
$s(n)$	noise-free signal
$x(n)$	noisy signal
S_i	transition span
$y(n)$	processed signal
ε	EMG denoising control parameter
$\phi_i(n)$	limiting threshold for the i^{th} decomposition level
$\gamma(n)$	time-varying thresholding factor
η	motion artifact denoising control parameter
μ	Mean
$\theta_i(n)$	time-varying threshold for the i^{th} decomposition level
σ	standard deviation

This page is intentionally left blank

Chapter 1
INTRODUCTION

1.1 Problem Overview

Electrocardiography is an important non-invasive diagnostic tool for identifying cardiac disorders. Electrocardiogram (ECG) is a record of the electric potentials generated by the currents causing the rhythmic contraction of the heart. Malfunction in the current generation or the conductive paths of these currents is generally manifested as an abnormality in the recorded ECG [1]–[3]. Artifacts may mask the visibility of certain important characteristic features. Further, the artifacts resembling one of the abnormal features in the ECG may lead to false diagnosis. The hardware used for ECG acquisition removes the noise present in the ECG recorded during the rest conditions, as in the case of cardiac monitoring in hospitals. But, many of the cardiac disorders may not be observable during rest state and it is important to analyze these cardiac signals recorded while performing normal day-to-day activities, i.e. ambulatory recording. An ambulatory recording is done using a wearable Holter monitor, which is a portable ECG recorder worn for continuous monitoring over an extended period. These ambulatory ECG signals are usually prone to noise and artifacts due to continuous movement of the patient's body and the attached electrodes. The presence of noise and artifacts in the ECG signals pose difficulties in getting its diagnostic information.

The nature and origin of the artifacts are of considerable interest, particularly for long term ambulatory monitoring. Some of the artifacts occur due to physiological reasons like electromyogram (EMG) noise caused due to voluntary or involuntary muscle activity in the body and slow baseline wandering due to respiration, whereas some artifacts occur due to non-physiological reasons like powerline interference and motion artifacts [5]. Motion artifact arises due to imbalance in the electrical activity at the electrode-electrolyte and electrolyte-skin interfaces caused by the motion of surface electrode. A plot of spectra of various components in the ECG is shown in Fig. 1.1. The ECG signals have their components in the

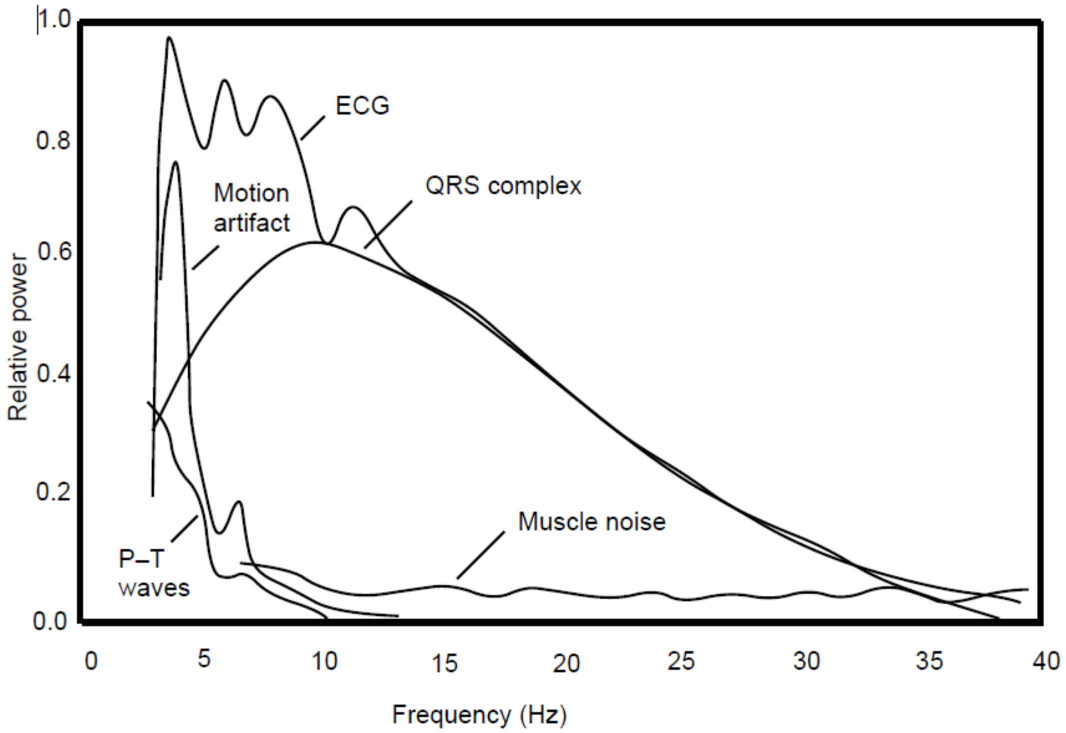

Fig 1.1 Relative power spectra of QRS complex, P and T waves, muscle noise and motion artifacts based on an average of 150 beats [1].

range of 0.05–150 Hz, with a 100 Hz bandwidth considered as valuable for diagnostic information [1], [4]. The baseline wander, EMG components and the motion artifacts extend over 0.01−1, Hz 5–500 Hz, and 1–10 Hz, respectively [1], [4]−[6].

Due the spectral overlap of the noise with that of the ECG, it is not possible to use linear filters for artifact suppression. EMG and motion artifact can be minimized by restricting the motion of the patient while recording. However, this is not feasible in an ambulatory ECG recording. Motion artifact is the most difficult form of noise to be eliminated from an ambulatory ECG as its spectrum completely overlaps with that of ECG and its morphology may resemble to that of P, QRS and T waves [15], [16]. ECG is a non-stationary signal with short lived components. The artifacts, motion artifacts, may be present only for a short duration; while some of them, like baseline wandering, may be present for a longer duration. Capturing and analyzing these artifacts requires an approach with good time and frequency resolution.

1.2 Project Objective

The objective of the project is to investigate wavelet based denoising techniques for suppression of EMG noise and motion artifact in ECG, and to extend the technique for different sampling frequencies of the input ECG. Level-dependent thresholding technique with improved thresholding function is used for suppression of EMG noise and coefficient limiting technique for motion artifact suppression. The effectiveness of the denoising technique is validated on ECG with simulated artifacts and on ECG acquired from patients with normal and abnormal cardiac conditions. Also, the robustness of the denoising technique to the variation of its noise parameters is studied. As wavelet based thresholding or coefficient limiting techniques have been reported to introduce ripples at the neighborhood of sharp transitions in the signal due to Gibbs phenomenon [35], [36], translation-invariant wavelet transform and stationary wavelet transform based implementations are investigated for the reduction of the effect of Gibbs phenomenon.

1.3 Outline of the Dissertation

Chapter 2 presents a review of the techniques reported for noise and artifacts suppression in ECG, the validation techniques, and ECG databases used for the investigation and validation. Chapter 3 gives a detailed description of the developed wavelet based denoising technique and its extension for different sampling frequencies. Investigations for reducing the denoising related distortions, using translation-invariant wavelet denoising and stationary wavelet transform based denoising are presented in Chapter 4. The next chapter gives the validation results of the denoising techniques for simulated noisy data, normal subject data and patient data. The last chapter gives a summary of the work done, conclusions, and some suggestions for future work.

This page is intentionally left blank

Chapter 2
DENOISING TECHNIQUES

2.1 Introduction

ECG is generally corrupted by baseline wander, EMG noise and motion artifacts. These noise and artifacts may mask the characteristic points of the signal, and thus introduce errors in the values of parameters estimated for clinical diagnosis. The presence of these artifacts is more prominent in ambulatory recording, and hence it is necessary to enhance the quality of the signals by suppressing these artifacts. Several denoising techniques such as digital filtering [7]−[11], adaptive filtering [12]−[18], independent component analysis [19], [20], empirical mode decomposition [21]−[23], and wavelet based denoising [24]−[38] have been reported for artifact suppression in ECG.

2.2 Digital Filtering

Alste and Schilder [7] designed an efficient FIR band-pass filter with reduced number of taps, which periodically adjusts its filter response, for removal of powerline interference and baseline wandering. The technique was investigated for ECG signals sampled at 250 Hz. Validation by visual inspection showed that the technique was able to remove baseline wander even from exercise ECG. It was reported to be ineffective in removing the baseline wander with the period close to that of the heartbeat and the processing occasionally suppressed ST segment depression and elevation.

Lee and Ben [8] proposed a variable bandwidth filter for denoising bio-signals with known boundaries in time-frequency domain. The filter was designed to adapt its cut-off frequency and bandwidth according to the short-time signal spectrum. It was reported that the filter rejected noise in the regions outside the short-time signal spectrum. It was tested on ECG signals recorded using a Holter monitor and an SNR improvement of 11 dB was obtained when compared to an LTI filter, and was not effective when the noise spectrum overlapped with the signal spectrum.

Dai and Lain [9] proposed the use of modified moving window averaging to estimate and remove the low-frequency baseline wander from ECG, by applying the moving average at specific time intervals. The filtering and moving window averaging techniques fail when there is a spectral overlap between the signal of interest and noise. Evaluation was carried out on noise-free ECG signals from MIT-BIH database with sampling frequency 360 Hz added with simulated baseline wander. Denoising using a simple moving average filter resulted in a correlation coefficient of 0.8543, while the use of modified moving average filter resulted in a value of 0.965.

Chouhan and Mehta [10] implemented baseline wander removal for multi-lead ECG, based on least mean square error correction and correction based on overall median of each lead. The QRS complexes were then detected to find the RR intervals and median based correction was applied for each of the RR interval to enhance the noise suppression. The technique was investigated for ECG signals from CSE ECG database for 125 records of 10 s each and sampling frequency of 500 Hz. The technique efficiently removed baseline wander and visual inspection showed that the ECG was not distorted. The main limitation of this technique is that R peak detection becomes difficult in the presence of high baseline wander or motion artifact. In [11], a varying-length moving averaging window technique was implemented for suppressing baseline wander and high frequency noise. The window was designed to exclude R peaks during the averaging process. The ECG signals from the PTB diagnostic ECG database were used for the investigation. The technique was also tested on ECG record 104 of MIT-BIH arrhythmia database by visual inspection. It was found that the technique was effective in suppressing the noise, but it may fail due to R-wave detection failures in the regions with high noise levels.

2.3 Adaptive Filters

Rahman *et al.* [12] proposed the use of normalized signal regressor LMS (NSRLMS) algorithm for artifact suppression. ECG of the MIT-BIH arrhythmia database (mitdb) and MIT-BIH normal sinus rhythm database (nsrdb) with added baseline wander (bw) and motion artifact (em) of MIT-BIH noise stress test database (nstdb) were used for validating baseline wander suppression and motion artifact suppression, respectively. For baseline wander, EMG noise, and motion artifact suppression with corresponding input SNR values of -21.5, 2.5 and 2.5 dB, SNR improvements of 7.34, 8.31 and 8.14 dB were obtained, respectively.

Tong *et al.* [13] used an adaptive filter for reducing motion artifact with a motion sensor as a reference input. LMS approach was used to adjust the weights of the adaptive filter. The ECG signals were recorded from 8 subjects under an IRB-approved protocol with sampling frequency 500 Hz. Three methods were used to introduce motion artifact on the electrode site − pushing the electrode, pinching the skin around the electrode and pulling the wires. L2 norm and MaxMin statistics were used for measuring the performance. It was reported that the reference from a tri-axial accelerometer performed better than the signal from 2-axis magneto-resistive motion sensor. It was also reported that improvement index values of 0.84 and 0.59 were obtained for L2 norm and MaxMin, respectively.

Jeong and Kim [14] reported that steepest decent algorithm for adapting the filter weights performed better than LMS approach. Evaluation was carried out by visual inspection of power spectral density of the input and denoised signals for 20 s duration ECG recordings from 7 healthy subjects. Sayadi and Shamsollahi [15] used extended Kalman filter for ECG denoising and compression. Artifact-free ECG signals from MIT BIH databases – mitdb and nsrdb – were used. Muscle artifacts (ma) and electrode motion (em) of MIT-BIH noise stress test database (nstdb) were added to the artifact-free ECG to obtain noisy ECG. SNR improvements of 10.16, 9.53 and 8.75 dB were obtained for input SNR of -5, 0 and 5 dB, respectively.

In [16], an adaptive recurrent filter structure was proposed for noise cancellation and arrhythmia detection. The adaptive filter minimizes MSE between noisy ECG and reference signal, and a two-stage filter was used to remove baseline wander, powerline interference, and motion artifact. It was reported to be superior to conventional adaptive filtering. The technique was prone to failing in the presence of high heart-rate variability or a gradual variation in the QRS morphology, preventing complete adaptation of the filter coefficients. It also required proper temporal coincidence between the reference signal and input signal. It was reported that large non-stationary motion artifacts that overlap with the QRS complex could not be suppressed due to the relatively slow convergence time of the adaptive filter. The filter was reported to produce minor distortions in the ECG signals limiting its application to rhythm analysis in ambulatory monitoring.

Sameni *et al.* [17] proposed a non-linear Bayesian adaptive filter framework for denoising single channel ECG. Noise-free ECG segments (190 segments, each of 30s duration) from MIT-BIH normal sinus rhythm database with sampling frequency 128 Hz were used for the investigation. Real muscle artifact (ma) from MIT-BIH noise stress test database with sampling frequency 360 Hz was resampled at 128 Hz and added to the noise-free ECG to get noisy signals. SNR Improvements (± standard deviation) of 12 (± 1.5), 11 (± 2), 9 (± 2.6), 6 (± 3.5) and -1 (± 4.9) dB were obtained for input SNR of -5, 0, 5, 10 and 30 dB, respectively. It was reported that this adaptive filter might fail when abnormal waves appear in certain cycles of ECG. Problems of convergence-time, stability, estimation bias and preciseness of filter results were also reported.

In [18], a normalized adaptive neural filter (NANF) was proposed for artifact cancellation. The filter coefficients were updated using steepest-descent error estimation technique, to minimize the error between second-order estimated output values and the desired artifact-free ECG signals. Seven ECG signals from MIT-BIH arrhythmia database (records 101, 103, 106, 116, 123, 202 and 232) with added muscle artifacts (record 'ma') from MIT-BIH noise stress test database were used as test signals. The RMS error and correlation coefficient of 0.07 and 0.9864 were obtained for LMS filter, while the corresponding values of 0.01 and 0.9997 were obtained for NANF. In terms of SNR, the NANF achieved an average of 35.53 dB, which was about 19.23 dB higher than the corresponding result with the LMS filter.

2.4 Independent Component Analysis (ICA)

Barros *et al.* [19] used ICA for eliminating muscle, motion, and respiratory artifacts from ECG. A self-adaptive step size and a two-layer neural network were implemented to estimate the mixing parameters. The noisy ECG data used for validation was obtained by mixing artifact-free ECG and ECG-free artifact signals from MIT-BIH noise stress test database. Validation by visual inspection showed that ICA performed better when compared to digital filtering techniques. Foresta *et al.* [20] proposed an ECG denoising technique which combined the properties of wavelets with ICA. The proposed technique was tested on multichannel ECG signals. A correlation coefficient value of 0.9 was obtained between the artifact-free and denoised ECG.

2.5 Empirical Mode Decomposition (EMD)

Velasco *et al.* [21] used EMD based denoising technique for suppression of baseline wander and EMG noise. The ECG records 100, 103, 105, 119 and 213 of MIT-BIH arrhythmia database were used. The signal-free artifacts, em and ma, from MIT-BIH noise stress test database was added to the artifact-free ECG signals to generate noisy ECG. For input SNR of 6, 10 and 14 dB, the output SNR values of 10.24, 13.08 and 15.74 dB were obtained, respectively. The technique was also reported to be effective in denoising of Holter monitor ECG signals.

An ECG denoising technique which employed EMD and wavelet adaptive thresholding was implemented in [22]. Adaptability of EMD was used to choose the wavelet function and wavelet thresholding was used to prevent the distortion introduced due to EMD based ECG denoising. The output SNR of 87.03, 79.22 and 82.83 dB, and mean square error (MSE) of 0.10776, 0.01306 and 0.01305 were obtained for EMD, wavelet and EMD-wavelet based denoising, respectively. Visual inspection of the denoised signals showed that a higher SNR with a lower MSE could be obtained when the signal is severely distorted resulting in reduction of its L2 norm of the signal. Tang and Qin [23] used EMD for noise wide band noise suppression. Artifact-free ECG records 100, 101,103 and 213 of MIT-BIH arrhythmia database were added with Gaussian noise to generate test signals. It was reported that denoising using EMG resulted in an output SNR of 14.82, 17.61, 19.21, and 20.03 dB for input SNR values of 6, 10, 14, and 16 dB, respectively.

2.7 Discrete Wavelet Transform (DWT)

The applicability of wavelets for denoising ECG signals has been studied extensively, due to its unique property of access to both time and frequency contents simultaneously. Several techniques using different wavelet shapes and thresholding have been studied. Proper selection of wavelet function and thresholding technique is considered to be important for efficient suppression of artifacts [25]. Also, the shape of the wavelet function selected should be either similar to the ECG signal or the artifact or noise. Daubechies, Coiflets, Symlets and bi-orthogonal wavelets were primarily used for ECG denoising.

Zhang [24] proposed a wavelet-based baseline wandering correction technique. For a sampling rate of 360 Hz, Ten-level decomposition with symlet-10 (sym10) was used due to its close similarity to QRS complex. The sampling frequency of the ECG signals determines the maximum number of decomposition levels to be used. It was reported that the coefficients of the eighth- level approximation corresponded to the low frequency drift in the baseline, but the high frequency components of the drift were not captured. Wavelet shrinkage (soft thresholding) was applied to remove the high frequency components of the baseline wander. The technique was investigated on ECG signal from record 118 of MIT-BIH arrhythmia database with baseline wander added from the record 'bw' from MIT-BIH noise stress test database. Visual inspection showed that the method removed baseline wander.

Kania *et al.* [25] studied the importance of the proper selection of mother wavelet with appropriate number of decomposition levels for reducing the noise content in high resolution multi-lead ECG signals. Soft thresholding with universal threshold was applied on the detail wavelet coefficients at each level. The efficiency of Daubechies (db1, db2, db3, db4, db5, db6, db7, db8), and symlet wavelets (sym2, sym3, sym4, sym5, sym6, sym7, sym8) as well as biorthogonal wavelets (bior3.3, bio4.4, bio6.8) were compared using visual inspection. The best wavelet was chosen according to the perseveration of the signal morphology. It was reported that db1 (for 4th and higher decomposition levels), sym3 (for 4th level) and sym8 (for 4th decomposition level) had given the best results for ECG denoising.

Singh and Tiwari [26] studied the performance of different wavelets (Daubechies of order 4, 6, 8, 10, 12; Symlet of order 4, 5, 6, 7, 8; Coiflet of order 1, 2, 3, 4, 5) on denoising and reported that db8 preserves the peaks of the ECG signal, which contains valuable physiological information for diagnostic purpose. The ECG data from biological signal processing (BSP) demonstration database with sampling frequency 500 Hz was used for the investigation. It was reported that db8 with Hybrid SURE shrink based denoising resulted in a lower RMS error, when compared to other wavelets. It was also reported that the error in detection of QRS was reduced to 5% for the denoised ECG from a corresponding value of 27% for noisy ECG.

Agante and Marques-de-Sá [27] used soft thresholding based on Donoho's statistical estimator and sliding window method for suppressing white Gaussian noise and powerline interference. The highly uncorrelated random noise like EMG noise and thermal noise were approximated to be white Gaussian noise. For a sampling frequency of 500 Hz, detail coefficients D1 corresponded to EMG and powerline frequency was located in D3. Soft thresholding was applied to the appropriate detail corresponding to the signal and the coefficients were reconstructed by climbing up the decomposition tree. The sliding window method of threshold estimation was reported to be more efficient over Donoho's statistical threshold estimation. ECG signals form CSE European database were used for investigation. The performance of the technique with Daubechies, Coiflet, and bi-orthogonal wavelets, were compared. Correlation coefficient (r) between the original ECG signal and denoised ECG was estimated to validate the performance of the wavelet for the QR, R peak, and RS regions. It was shown that biorthogonal wavelets preserve QR and R peak regions with an r value of 0.998, while distort the RS region with an r value of 0.797. It was also reported that Coiflet and Daubechies show similar performances with r value of 0.999, 0.996 and 0.986 for QR, R peak and RS regions, respectively.

Tinati and Mozaffary [28] proposed wavelet packet approach for baseline drift cancellation. The ECG records 103, 105, 115 and 210 of MIT-BIH arrhythmia database were used for the investigation. A sine wave of 0.01 Hz was added to the artifact-free ECG signals to generate noisy ECG signals with input SNR of -5 dB. A percentage RMS difference (PRD) value of 1.99 % was obtained for the denoised signal, indicating a good performance of the technique for baseline wander suppression. Cherkassy and Kilts [29] applied wavelet denoising to suppress EMG noise from ECG signals The accuracy and robustness of several thresholding methods based on VISU, SURE and soft thresholding, were compared with a new thresholding approach based on Vapnik-Chervonekis (VC) learning theory. When applied on ECG with EMG noise, VC based denoising resulted in mean square error (MSE) of 7.77 %, 8.72 %, and 0.56 % less than that of VISU, SURE and soft thresholding.

Pooranachandhra [30] proposed sub-band adaptive thresholding technique for removal of white additive Gaussian noise from ECG. 50 ECG signals (30 patients with normal and abnormal cardiac conditions) from MIT-BIH arrhythmia database with sampling frequency 360 Hz were used for the investigation. The performance of S-median threshold based estimation was compared with universal and minimax thresholds. In terms of SNR, for noise level of 10% (43.94 dB), the output SNR of 25, 26 and 27 dB were obtained for universal, minimax and S-median thresholds, respectively. The SNR degradation may be attributed to the distortion introduced due to processing. For 50 % noise level (0 dB SNR), the corresponding output SNR values of 15, 17 and 20 dB were obtained. These results indicated that noise suppression was much stronger when compared to small levels of distortions. For noise level of 90% (-43.94 dB), the corresponding output SNR values of 10.5, 11 and 14 dB were obtained. The results indicate that S-median based method introduced less distortion and also resulted in better denoising.

Tikkanen [31] studied the performance of wavelet and wavelet packet based denoising for removing simulated noise from ECG. 50 noisy ECG data with input SNR of 5 dB were generated by adding Gaussian noise, uniform white noise and non-white noise (using 4th order auto-regressive filter) to artifact-free ECG recorded with sampling frequency 512 Hz. Validation using RMS errors showed that about 50% of error is localized in the QRS due to soft thresholding and wavelet based denoising performed better than wavelet packet based denoising. The wavelet packet approach showed higher standard deviation in RMS values indicating higher performance variation for different ECG signals.

Sharma *et al.* [32] proposed a denoising technique based on the evaluation of higher-order statistics at different wavelet bands of decomposed ECG. The higher-order statistics, kurtosis and the energy contribution efficiency were used as indicators of the noise content in the signal. The technique was implemented for noisy multichannel ECG signals from 12-lead data of standard ECG database, CSE mutli-lead measurement library with sampling frequencies, 360 Hz, 500 Hz and 1000 Hz. It was observed that the denoising scheme filtered the signal effectively and retained the diagnostic information. For ECG with real noise (dataset M01-003), denoising using soft thresholding resulted in a percentage RMS difference (PRD) of 1.1 % and wavelet weighted PRD (WWPRD) of 1.60 %, while denoising using the proposed method resulted in the corresponding values of 7.4 % and 15.71 %. It was reported that wavelet energy-based diagnostic distortion measure (WEDD) could be used to distinguish between the increase in error between the noisy and denoised signal due to higher efficiency of proposed technique and the increase in error due to increase in induced distortions. The WEDD value was obtained as 1.94 % for soft thresholding and 1.87 % for the proposed method, showing that the lower WEDD was due to improved retention of morphological features of ECG.

Mithun [33] investigated the use of wavelet based denoising with different wavelet functions for suppression of baseline wander. Artifact-free ECG signals from MIT-BIH arrhythmia database were added with noise signals from MIT-BIH stress test database. The performance of the wavelet functions were estimated using SNR improvement and RMS error statistics. It was reported that discrete Meyer wavelet showed best SNR improvement for denoising and least RMS error for reconstruction. In [34], improved thresholding function for suppression of EMG noise and coefficient limiting technique for suppression of motion artifacts was proposed. Ten-level decomposition was applied for the ECG signal sampled at a frequency of 360 Hz. The approximation coefficients A_{10} were set to zero for suppressing the baseline wander. It was reported that the detail coefficients D_1−D_4 contained the EMG noise components. The coefficients D_2−D_5 (for sampling frequency 360 Hz) were modified using a modified thresholding technique, combining the features of hard thresholding and soft thresholding. The thresholds for each level were estimated from the statistics of coefficient values of D1. As D1 had insignificant ECG components, it was set to zero. For motion artifact suppression, hard limiting was applied on detail coefficients on the non-zero levels. The thresholds for hard thresholding were estimated from noise-free segment of ECG. If a noise-free segment was not located, the values were estimated using noise statistics of the ECG. For input SNR of -5, 0 and 5 dB, SNR improvements of 11.4, 8.3 and 4.9 dB were reported. It was also reported that the values of L2 norm and MaxMin based improvement indices were close to one indicating efficient denoising with significant distortion of the ECG. Performance evaluation based on R peak detection resulted in 12.3 % (54 failures and 14 false detections) error and 1.5 % (4 failures and 4 false detections) error, before and after denoising, respectively. The method could also be applied on signals with sampling rate of 200 Hz with an appropriate selection of levels.

The research was taken further in [35] and two modified thresholding functions, with exponential and sinusoidal transition, were proposed for EMG suppression, while three soft limiting functions with piece-wise linear, sinusoidal and parabolic transition were proposed for motion artifact suppression. For input SNR of -10, 5, 0 and 5 dB, the L2 norm improvement index was observed to be 1.1, 1.2, 1.5 and 2.2, respectively, while MaxMin improvement index was observed to be 1.2, 1.6, 3.9 and 11.8, respectively. Performance evaluation based on R peak detection for noisy ECG with simulated artifact resulted in 13 % failure (1.5 % false) and 2 % failure (0.2 % false) error, before and after denoising, respectively. Performance evaluation based on R peak detection for ambulatory ECG resulted in 9.8 % failure (2.5 % false) and 0.7 % failure (% 0.7 false), before and after denoising, respectively. It was also reported that wavelet thresholding resulted in ripples at sharp transitions in the signal due to Gibbs phenomenon, and that it could be reduced by using translation-invariant denoising.

2.8 Translation-invariant Wavelet Transform (TIWT) and Stationary Wavelet Transform (SWT)

Translation-invariant denoising was implemented in [36] to denoise ECG. Symlet-8 with 4-level decomposition was used to remove EMG noise from ECG. The MIT-BIH ECG database with sampling frequency 360 Hz and signal length of 1024 was used for validation of the technique. The performances of hard, soft and an improvised thresholding using DWT and TIWT were compared. For an input SNR of 17.08 dB, the output SNR values for DWT with hard, soft and improvised thresholding were obtained as 21.37, 19.04 and 21.97 dB, while that of TIWT were 23.23, 20.44 and 23.33 dB, respectively. The improvement in SNR was attributed to the reduction in the effect of Gibbs phenomenon in the Q and S waves.

Li e*t al.* [37] used stationary wavelet transform based denoising for suppression of baseline wander, EMG noise, motion artifacts and powerline interference in the ECG signals, using symlet 4 and 5-level wavelet decomposition.. The ECG signal from MIT-BIH arrhythmia database, record 100, was mixed with the artifacts, bw, em, ma, from MIT-BIH noise stress test database. The SNR improvement for hard shrinkage function with EBayes threshold was estimated for different input SNR. For SNR varying from 1 dB to 10 dB, The performance for decomposition were compared for level 3 to level 8 and the best results were obtained for level 5 with output SNR varied from 11.6 to 20 dB. It was also reported that for the ECG signal from record 104 of nstdb, the SNR output of 1.1, 0.9 and 0.6 dB was obtained for input SNR values of -13.1, -19.0 and -22.6 dB.

In [38], the performance of wavelet packet (WP), lifting wavelet (LW) and SWT were compared. The ECG signals from MIT-BIH database were used as test signals. Wavelet shrinkage was applied for 5-level wavelet decomposition using symlet 8. For an input SNR of

-32.46 dB, the output SNR values of -1.26, -1.23 and 0.52 dB were obtained for WP, LW and SWT based denoising, respectively. The corresponding output SNR values were 3.86, 2.54 and 4.49 dB for an input SNR of 0.6035, respectively.

2.10 Summary

Several methods such as digital filtering, ensemble averaging, adaptive filtering, ICA, EMD and wavelet based denoising techniques have been reported for artifact and noise suppression in ECG. Linear filters are not very effective in denoising ECG due to spectral overlap between the noise and ECG components. Also, they induced distortions in the signal, especially in the ST segments, which is an important feature for the diagnosis of ischemia and myocardial infarction. The amplitude of QRS complex of the ECG was also found to be reduced in some cases. Adaptive filtering technique was found to be effective in motion artifact suppression when a reference electrode motion signal is available. ICA was found to be computationally inefficient. In EMD based denoising, the band limits of the decomposition depend on the noise content of the signal, and hence, it cannot be used for designing a uniform denoising technique. Wavelet based denoising techniques were found to be very effective when applied along with proper thresholding or clipping techniques and appropriate decompositions.

Chapter 3
ARTIFACT SUPPRESSION IN ECG

3.1 Introduction

This chapter presents a wavelet based denoising technique for suppression of baseline wander, EMG noise, and motion artifacts. Level-dependent thresholding is used for suppression of EMG noise and coefficient limiting is used for suppressing motion artifact with thresholds estimated using the statistics of the noisy signal. All the analysis and processing are carried out using Matlab. A description of the denoising technique is given in Section 3.2. The effect of sampling frequency on the denoising technique is presented in Section 3.3. The results are presented and discussed in Section 3.4.

3.2 Suppression of Baseline Wander, EMG noise and Motion Artifacts

Several wavelet based ECG denoising methods have been reported in [24]−[38]. Wavelets have a unique property of time-frequency representation which can be used to capture noise present at a specific time and in a specific spectral band. In wavelet denoising, selection of the appropriate wavelet basis is very important. To capture the artifacts and noise in ECG, the shape of the wavelet (or its scaling function) should be similar to that of the ECG, as the noise and artifacts do not have a definite shape.

The implementation of discrete wavelet transform based ECG denoising of ECG is shown in Fig. 3.1. For input signal sampled at 360 Hz, eight-level discrete wavelet decomposition of input ECG is applied to obtain detail coefficients $D_1 - D_8$ and approximate coefficients A_8. The slow baseline wander which is captured in A_8 is suppressed by setting the approximate coefficients to zero. The EMG noise and motion artifacts are suppressed using non-linear modifications of the detail wavelet coefficients as described in the following two subsections.

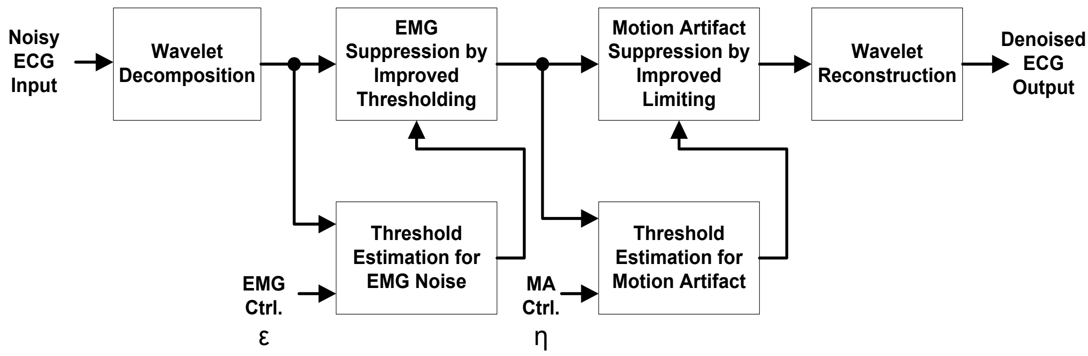

Fig. 3.1 DWT based denoising of ECG.

3.2.1 Suppression of EMG Noise

EMG is a non-stationary broadband noise superimposed on ECG signal due to voluntary and involuntary muscle activities occurring in the body. In case of ECG corrupted with ECG noise, the noise is always present and is of lower amplitude when compared to ECG which is of relatively higher amplitude. Hence, thresholding of the wavelet coefficients can be used to EMG suppression. The suppression of EMG in ECG signals involves two steps: threshold estimation and thresholding of wavelet coefficients. The EMG noise is manifested only in lower scales of wavelet decomposition. For a sampling frequency of 360 Hz, the EMG noise is predominantly represented in details $D_1 - D_5$ and particularly in D_1 and D_2. In threshold estimation stage, a time-varying threshold θ_i is estimated from the detail coefficients D_1 and D_2 (upsampled and added to D_1) and it is resampled to match the number of samples in each scale.

The technique proposed in [34] and [35] is used as a base for further improvisation. The absolute value of the combined details D_{th} (obtained from D_1 and D_2) is high in segments corresponding to QRS complexes or with significant EMG noise. A time-varying threshold thus obtained is resampled to match the number of samples in D_i. Since the duration of QRS complex is shorter than the typical EMG bursts, D_{thLP} was obtained by applying a 35-point moving average filter on $|D_{\text{th}}|$ to suppress the values corresponding to the QRS complexes. The time-varying threshold $\theta_i\big|_{i=3,4,5}$ is obtained as.

$$\theta_i(n) = \varepsilon\gamma(n)\rho 90\left[\left|D_i(n)\right|\right] \tag{3.1}$$

where $\rho 90\left[\left|D_i(n)\right|\right]$ is the 90th percentile of $D_i(n)$, $\gamma(n)$ is a time-varying thresholding factor obtained from $D_{\text{thLP}}(n)$ and ε is the EMG denoising control parameter. The extent of noise suppression is controlled by an empirically set value for ε. Too high a value of ε may introduce distortions in the denoised ECG. 90th percentile of $D_i(n)$ is chosen to reduce the effect of overshoots induced by the anti-aliasing filter of the resampling operation on the estimated threshold. The time-varying thresholding factor $\gamma(n)$ is calculated from $D_{\text{thLP}}(n)$ as

$$\gamma(n) = \begin{cases} 0, & D_{\text{thLP}}(n) < D_{\text{th}\rho 5} \\ \dfrac{D_{\text{thLP}}(n) - D_{\text{th}\rho 5}}{D_{\text{th}\rho 95} - D_{\text{th}\rho 5}}, & D_{\text{th}\rho 5} \le D_{\text{thLP}}(n) \le D_{\text{th}\rho 95} \\ 1, & D_{\text{thLP}}(n) > D_{\text{th}\rho 95} \end{cases} \tag{3.2}$$

The lower threshold, $D_{\text{th}\rho 5}$ is taken as 5th percentile of D_{thLP} and the upper threshold, $D_{\text{th}\rho 95}$ is taken as half of the 95th percentile of D_{thLP}. 5th percentile of D_{thLP} is an optimum value chosen to reduce the magnitude of the threshold for wavelet coefficients corresponding to noise-free ECG segments, while 95th percentile of D_{thLP} is chosen to have uniform threshold for wavelet coefficients corresponding to segments with high EMG noise. This is to ensure uniform EMG suppression in the regions with significant EMG noise and avoid shape change introduced due to non-uniformity. In thresholding stage, a sinusoidal thresholding technique developed by combining characteristics of soft and hard thresholding was applied on details $D_3 - D_5$. The sinusoidal thresholding function is given as

$$\hat{D}_i(n) = \begin{cases} 0, & |D_i(n)| < \theta_i(n) \\ \dfrac{D_i(n)}{2}\left[1 - \cos\left(\dfrac{\left(|D_i(n)| - \theta_i(n)\right)\pi}{S_i}\right)\right], & \theta_i(n) \le |D_i(n)| \le \theta_i(n) + S_i \\ D_i(n), & |D_i(n)| > \theta_i(n) \end{cases} \tag{3.3}$$

The function approximates soft thresholding for input coefficients lower than $\theta_i(n)$ and approximates hard thresholding for values higher than $\theta_i(n) + S_i$. For reduction of the EMG noise, S_i is empirically chosen to be 95th percentile of $D_i(n) - \theta_i(n)$ values where $|D_i(n)| > \theta_i(n)$ to ensure maximum EMG reduction with minimum signal distortion. The coefficients used for estimating the threshold (D_1 and D_2) were set to zero during reconstruction as it predominantly contains EMG noise.

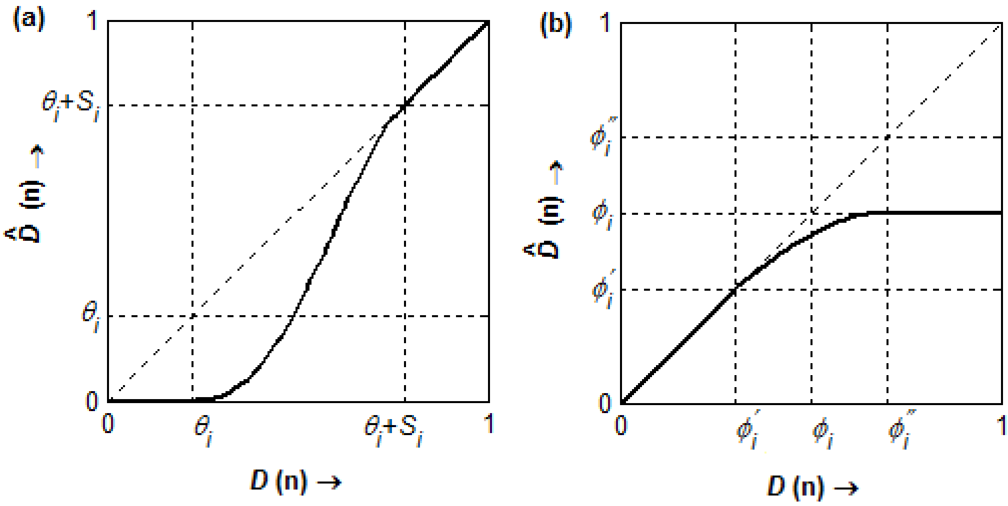

Fig. 3.1 Coefficient thresholding and limiting: (a) sinusoidal thresholding function and (b) sinusoidal soft-limiting function [35].

3.2.2 Suppression of Motion Artifact

The main assumption of most of the noise suppression techniques based on wavelet thresholding is that the noise is always present and has low amplitude, while the signal is present in specific time segments and has relatively high amplitude [39]. In case of ECG corrupted with non-stationary motion artifact, ECG signal is always present and motion artifacts occur only intermittently and have generally higher amplitudes when compared to that of ECG. Hence, limiting of wavelet coefficients can be used for motion artifact suppression [34]. For an automated operation, the parameters for limiting are statistically obtained from the signal itself.

The suppression of motion artifact is carried out in two stages – threshold estimation and limiting of wavelet coefficients. Since the estimated threshold should be high enough to exclude the possibility of reducing the artifact-free ECG and low enough to suppress the motion artifact, the thresholds are estimated by dividing the ECG record into segments of two cardiac cycles. The limiting threshold ϕ_i for a scale i is calculated as $\phi_i = \mu_i - \eta\sigma_i$, where η is a motion artifact denoising control parameter and is empirically set, μ_i and σ_i are the mean and standard deviation, respectively, of the maximum absolute values of coefficients in the segments. A value of η close to 0.5 has been found to result in effective denoising without distortion. A larger value can be used for signals with very large motion artifacts, but it can result in distortion in the artifact-free ECG segments. A sinusoidal coefficient limiting function obtained by combining hard limiting and soft limiting techniques as given by eq. 3.4 was applied on details $D_3 - D_8$.

$$\hat{D}_i(n) = \begin{cases} D_i(n), & |D_i(n)| < \phi_i' \\ \operatorname{sgn}\left(D_i(n)\right)\left(\phi_i' + \left(\phi_i - \phi_i'\right)\sin\left(\dfrac{\left(|D_i(n)| - \phi_i'\right)\pi/2}{\left(\phi_i'' - \phi_i'\right)}\right)\right), & \phi_i' \le |D_i(n)| \le \phi_i'' \\ \operatorname{sgn}\left(D_i(n)\right)\phi_i, & \phi_i'' < |D_i(n)| \end{cases} \quad (3.4)$$

where $(\phi_i - \phi_i')/(\phi_i'' - \phi_i) = 2/\pi$, ϕ_i' and ϕ_i'' are two additional thresholds used for incorporating a smoother transition between them. The coefficients below the threshold ϕ_i' remain unmodified, while the coefficients above ϕ_i'' are limited to ϕ_i. The coefficients lying between the thresholds ϕ_i' and ϕ_i'' are modified using a function having a transition from ϕ_i' to ϕ_i''. The above mentioned limiting thresholds for each scale can be obtained from the noisy ECG itself or from artifact-free segment of the ECG signal.

3.3 Decomposition levels for Different Sampling Frequencies

Since wavelet based denoising technique involves capturing time and frequency features, sampling frequency of the input ECG is important. For different sampling frequencies, noise and artifacts are expressed in different scales. Resampling the signals to 360 Hz and applying artifact suppression technique may not be effective as some important diagnostic points may be affected due to the anti-aliasing filter of the resampling operation. Hence, the denoising technique has to be adapted for different sampling frequencies. The number of decomposition levels and the scales used for suppression of EMG and motion artifacts are chosen according to the scales corresponding to the spectrum of the EMG and motion artifacts and by RMS error based investigation. Table 3.1shows the total number of decomposition levels applied, the detail scales used EMG suppression and the detail scales used for motion artifact suppression for sampling frequencies from 100 Hz – 500 Hz in steps of 10 Hz.

For sampling frequencies 128 and 150 Hz, seven-level decomposition was used and A_7 was set to zero for baseline wander suppression. The thresholds were estimated from detail coefficients D_1 for EMG suppression and modified thresholding was applied on detail coefficients D_1 - D_3 for EMG suppression. For sampling frequency of 200 Hz, seven-level

Table 3.1 Number of decomposition levels and scales used for EMG and motion artifact suppression for different sampling frequencies.

Sampling frequency (Hz)	No. of decomposition levels	Scales used for EMG threshold estimation	Scales used for EMG suppression	Scales used for MA suppression
100−115	6	D_1	D_1−D_3	D_2−D_6
116−179	7	D_1	D_1−D_3	D_2−D_7
180−230	7	D_1	D_2−D_4	D_2−D_7
231−287	8	D_1	D_2−D_4	D_2−D_7
288−359	8	D_1	D_2−D_4	D_2−D_7
360−460	8	D_1, D_2	D_3−D_5	D_3−D_8
461−500	9	D_1, D_2	D_3−D_6	D_3−D_9

decomposition was used and A_7 was set to zero for baseline wander suppression. The thresholds were estimated from detail coefficients D_1 for EMG suppression and $D_1$was set to zero. Modified thresholding was applied on detail coefficients D_2 – D_4 for EMG suppression. For motion artifact suppression, coefficient limiting was applied on for details D_2 – D_7 with thresholds estimated from respective scales. For sampling frequencies of 250 and 360 Hz, eight-level decomposition was used and A_8 was set to zero for baseline wander suppression. Detail coefficients D_1 and D_2 were used to the thresholds EMG suppression and the coefficients were set to zero. Modified thresholding was applied on detail coefficients D_3 – D_5 for EMG suppression. For motion artifact suppression, coefficient limiting was applied on for details D_3 – D_8 with thresholds estimated from respective scales. For sampling frequencies of 500 Hz, nine-level decomposition was used and A_9 was set to zero for baseline wander suppression. The thresholds were estimated from detail coefficients D_1 – D_3 for EMG suppression and D_1 – D_3 were set to zero. Modified thresholding was applied on detail coefficients D_3 – D_6 for EMG suppression. For motion artifact suppression, coefficient limiting was applied on for details D_3 – D_9 with thresholds estimated from respective scales.

3.4 Results and Discussion

Wavelet based denoising techniques were investigated for the suppression of EMG noise and motion artifacts in ECG. EMG noise was reduced by modified thresholding, combining the

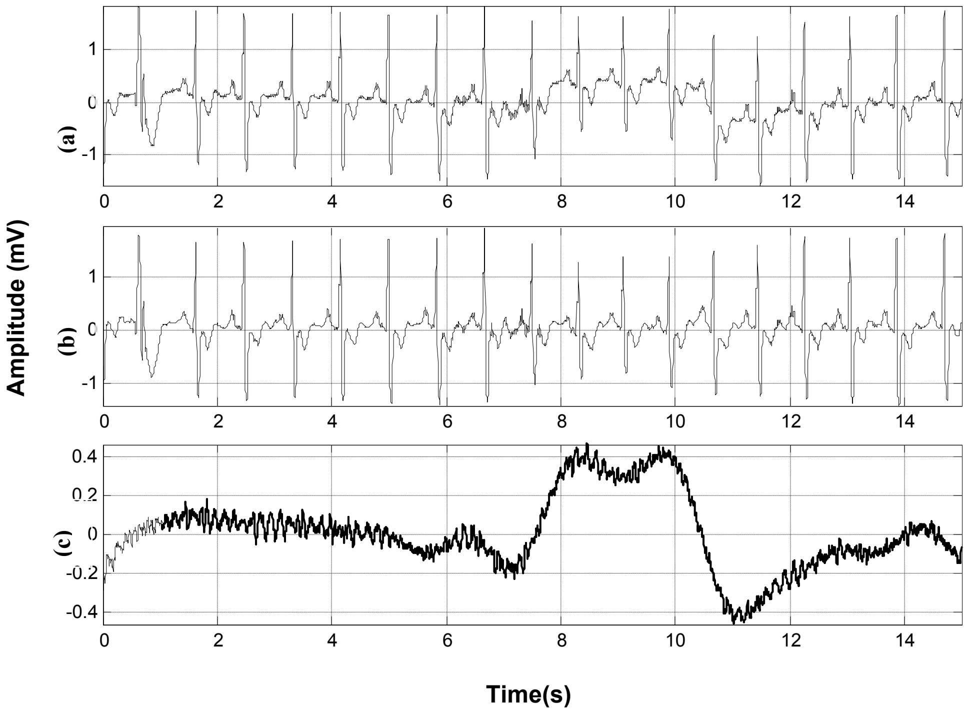

Fig 3.3 Suppression of EMG noise in ECG using level-dependent thresholding: (a) ECG signal corrupted with baseline wander and EMG noise, (b) denoised ECG, and (c) estimated baseline wander and ECG noise.

Fig 3.4 Suppression of motion artifacts in ECG using wavelet coefficient limiting: (a) ECG signal corrupted with motion artifact, (b) denoised ECG, and (c) estimated motion artifact.

features of hard and soft thresholding. Motion artifact was reduced by limiting the wavelet coefficients. Thresholds for both the denoising were estimated from the statistics of the noisy signal in an automated manner. The effect of discrete wavelet transform based denoising on the ECG signals corrupted with EMG and motion artifact is shown in Fig. 3.2 and Fig. 3.3, respectively. It can be seen that the denoising technique can effectively remove baseline wander, EMG and motion artifacts. The artifact-free segments are not affected much by for EMG suppression, but for motion artifact suppression the QRS complexes in the artifact-free ECG region are slightly attenuated. When thresholding or limiting is applied, ripples are formed in the neighborhood of QRS complexes due to the effect of Gibbs oscillations in the vicinity of sharp changes in the ECG signals. Translation-invariant wavelet transform and stationary wavelet transform based denoising are investigated for suppressing the effect of Gibbs phenomenon. Extensive qualitative and quantitative analysis of the denoising techniques on simulated noisy ECG signals are given in Chapter 6. The techniques are also validated on patient data with cardiac abnormalities and real-time artifacts from sudden cardiac death database and MIT-BIH ECG databases with sampling frequencies.

A LabWindows based application “ECG Denoiser, v.2” has been developed for artifact suppression technique in 8-bit ECG signals recorded using Holter monitor at a sampling rate of 200 Hz. The application involves wavelet based denoising applied on 3-Lead ECG. The user manual of the application is given in Appendix A.

Chapter 4
SUPPRESSION OF
DENOISING RELATED DISTORTION

4.1 Introduction

Thresholding and coefficient limiting techniques based on the discrete wavelet transform sometimes exhibits visual artifacts due the effect of pseudo-Gibbs phenomena in the neighborhood of sharp changes in the signals. This can be mainly seen as ripples being formed at Q and S parts of the QRS complexes of ECG. Also, due to thresholding, some undershoots or overshoots may appear in the other parts of the ECG signals which are corrupted by noise [40]. Two methods have been reported to suppress the effect of Gibbs phenomenon; (a) translation-invariant wavelet transform (TIWT) [36] and (b) undecimated or stationary wavelet transform (SWT) [37]−[38]. Investigations using translation-invariant wavelet transform and stationary wavelet transform are described in Sections 4.2 and 4.3, respectively. The results from the two methods are compared with DWT based denoising in Section 4.4.

4.2 Translation-Invariant Wavelet Denoising

The size and extent of localized Gibbs phenomenon, which is introduced by discrete wavelet transform based denoising, depends on the actual location of the sharp transitions and the number of sharp transitions in the ECG signal. If a sharp transition has an exact temporal alignment with the sharp transitions of the wavelet function, then no pseudo-Gibbs oscillations occur and the number and amplitude of oscillations increases with the increase in time difference between the location of sharp transition in the ECG signal and the wavelet function [40]. Thus, different temporal alignments of the same ECG signal with respect to the analysis window generate different oscillatory artifacts or even fewer ripples.

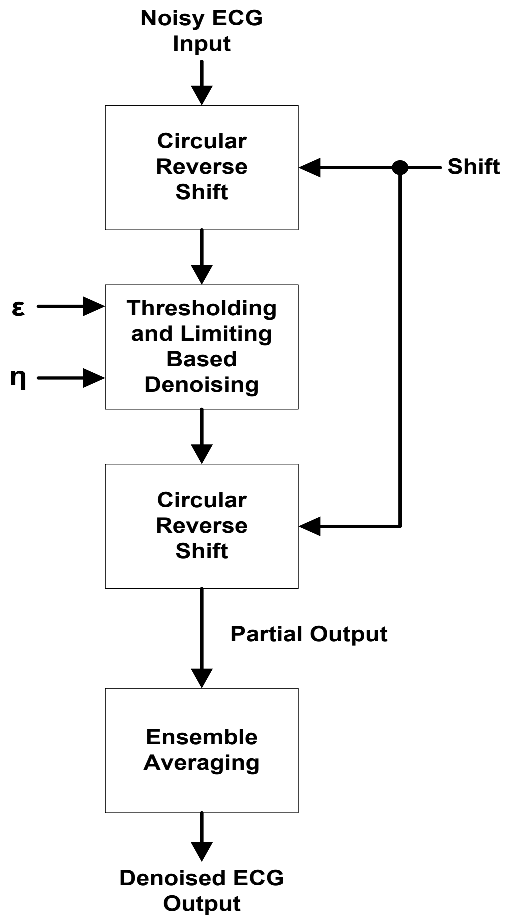

Fig. 4.1 TIWT based ECG denoising.

In TIWT processing, the input ECG signal is circular time-shifted and the traditional wavelet denoising is applied. The resultant denoised ECG is realigned to the original starting point by circular shifting in the opposite direction. For an ECG signal which contains several sharp transitions, the denoised ECG obtained from a specific alignment might give best result for one sharp transition and may have largest ripples for another sharp transition. Processing of the signal with different amounts of circular shifts and ensemble averaging of the resulting outputs is likely to suppress the ripples. The extent of suppression depends on the number of circular shifts applied. The implementation of TIWT ECG denoising is shown in Fig. 4.1.

For the investigation of TIWT based denoising, SNR is estimated with QRS and by subtracting QRS complex is applied for simulated ECG signals denoised using different number of circular shifts. The effect of number of circular shifts used in translation-invariant denoising on the output SNR when applied on artifact-free ECG and noisy ECG with SNR of 5 dB is shown in Fig. 4.2 and Fig. 4.3, respectively.

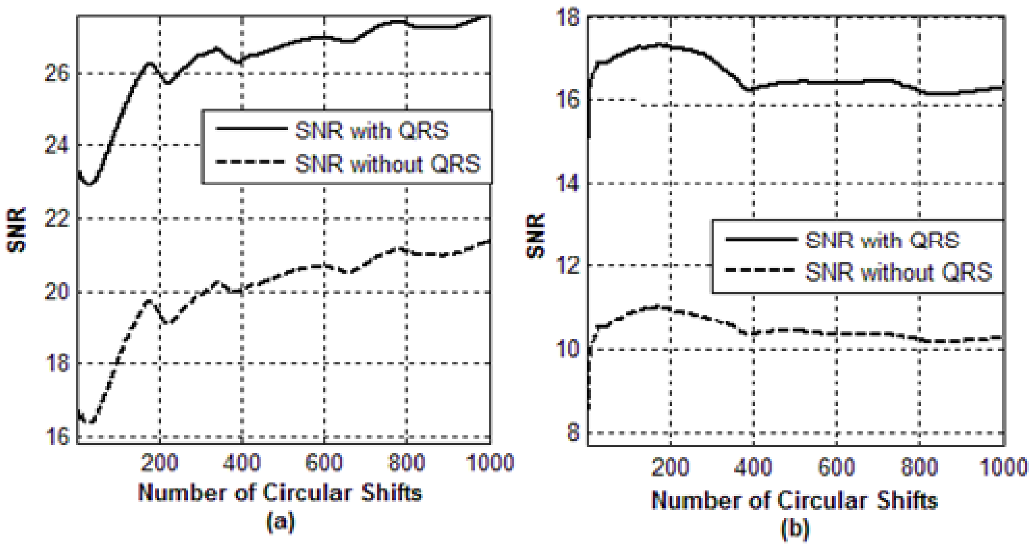

Fig. 4.2 Effect of number of circular shifts in TIWT based denoising: on output SNR for (a) artifact-free ECG and (b) noisy ECG with input SNR = 5 dB (-1. 7059 dB when estimated by subtracting QRS).

An overall increase of the output SNR with the increase in the number of circular shifts was observed. The exact variation of the SNR was found to depend upon the location and number sharp transitions in the ECG signal. To quantify the amount of distortion induced in ECG due to denoising, TIWT based denoising was applied on an artifact-free ECG signal of 10 s duration from MIT-BIH arrhythmia database with sampling frequency 360 Hz. For DWT based denoising (TIWT with zero circular shifts) on artifact-free ECG, an output SNR of 22.3 dB was obtained, where 6.5 dB corresponds to the QRS complex. This is mainly due to the ripples introduced in the neighborhood of the QRS complex. With increase in number of iterations for TIWT, the SNR improves due to decrease in the amount of induced distortions, as shown in Fig. 4.2.(a). A 4 dB increase in output SNR was be observed for 180 shifts. This shows that when compared to DWT, TIWT based denoising has lesser effect on artifact-free segment of EC. The processed output ECG signals are shown in Fig. 4.3 showing significant reduction in the number of ripples and ripple amplitude with increase in the number of circular shifts. When the change in output SNR estimated with QRS complex is compared with output SNR estimated by subtracting QRS complex, it can be observed that a similar pattern of SNR change occurred with a difference in SNR of about 6 dB. This indicates that effect of TIWT based denoising is mainly in the region outside the QRS complex, where the ripples are introduced by DWT based denoising and are suppressed by TIWT based denoising.

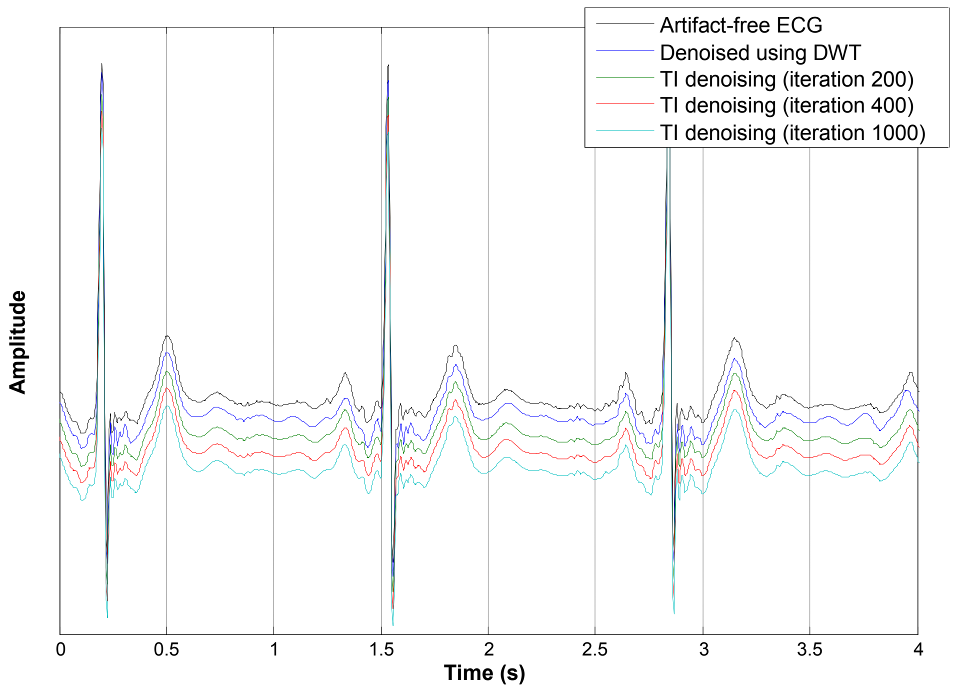

Fig. 4.3 Processed output from translation-invariant denoising applied on artifact-free ECG. (ECG amplitude in arbitrary units and shifted for non-overlapping plots of the waveform.)

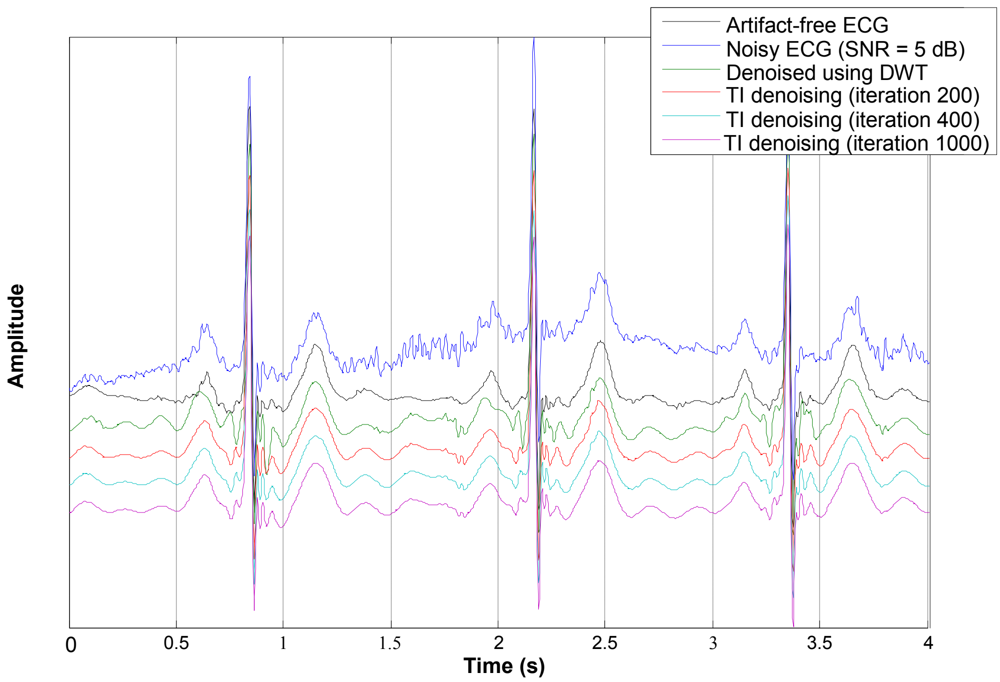

Fig. 4.4 Processed output from translation-invariant denoising applied on noisy ECG with input SNR of 5 dB. (ECG amplitude in arbitrary units and shifted for non-overlapping plots of the waveform.)

Table 4.1 Performance comparison of DWT, TIWT and SWT for artifact-free ECG and noisy ECG with SNR = 5dB (-1.7059 dB without QRS).

Wavelet Method	Output SNR for artifact-free ECG		Output SNR for noisy ECG	
	With QRS	Without QRS	With QRS	Without QRS
DWT	22.28	15.82	13.90	7.84
TI (n=200)	26.02	19.40	17.36	10.98
TI (n=400)	26.35	20.02	16.36	10.37
TI (n=1000)	27.61	21.37	16.38	10.26
SWT	24.51	17.88	18.44	11.95

Noisy ECG signals of SNR 5 dB are generated by adding ECG-free artifacts from records ‘bw’, ‘em’ and ‘ma’ of MIT-BIH noise stress test database to the artifact-free ECG signal. Application of DWT based denoising on the artifact-free ECG resulted in an output SNR of 22.3 dB. Excluding the QRS complexes, the output SNR was found to 15.8 dB, indicating that the distortion in the form of ripples occurred outside the QRS complexes.

When TIWT based denoising was applied to noisy ECG, a similar effect was seen as shown in Fig. 4.2.(b). An output SNR of 13.9 dB for input SNR of 5dB (from -1.71 dB to 7.8 dB when estimated by removing the QRS complex) was obtained for DWT based denoising due the ripples introduced in the sharp transitions in the neighborhood of the QRS complex. A steep increase in the SNR to 17.4 dB (and 11.0 dB without R-peak) is seen till 180 shifts, but after 180 shifts the effect of TIWT based denoising is seen to be deteriorating indicating that the misalignment between the sharp changes in ECG and the wavelet function is increased for circular shifts greater than 180 samples. This implies that proper estimation of number shifts implemented in the denoising technique is very important for effective ripple reduction. The processed output ECG signals are shown in Fig. 4.4. For different ECG signals which have different number and location of sharp transitions, the number of shifts required for maximum ripple suppression varies. When the change in output SNR estimated with QRS complex is compared with output SNR estimated by subtracting QRS complex, it can be observed that a similar pattern of SNR change occurred with a difference in SNR of about 6 dB. This indicates that the QRS complex is not affected by TIWT based denoising and the effect is mainly in the region outside the QRS complex.

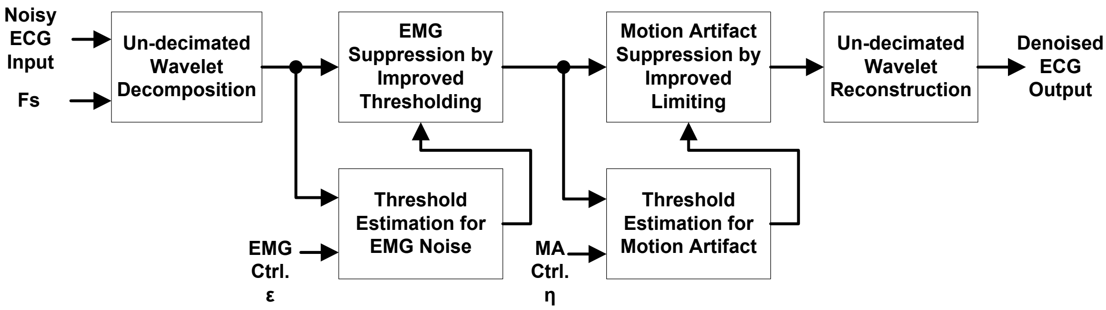

Fig. 4.5 SWT based denoising of ECG.

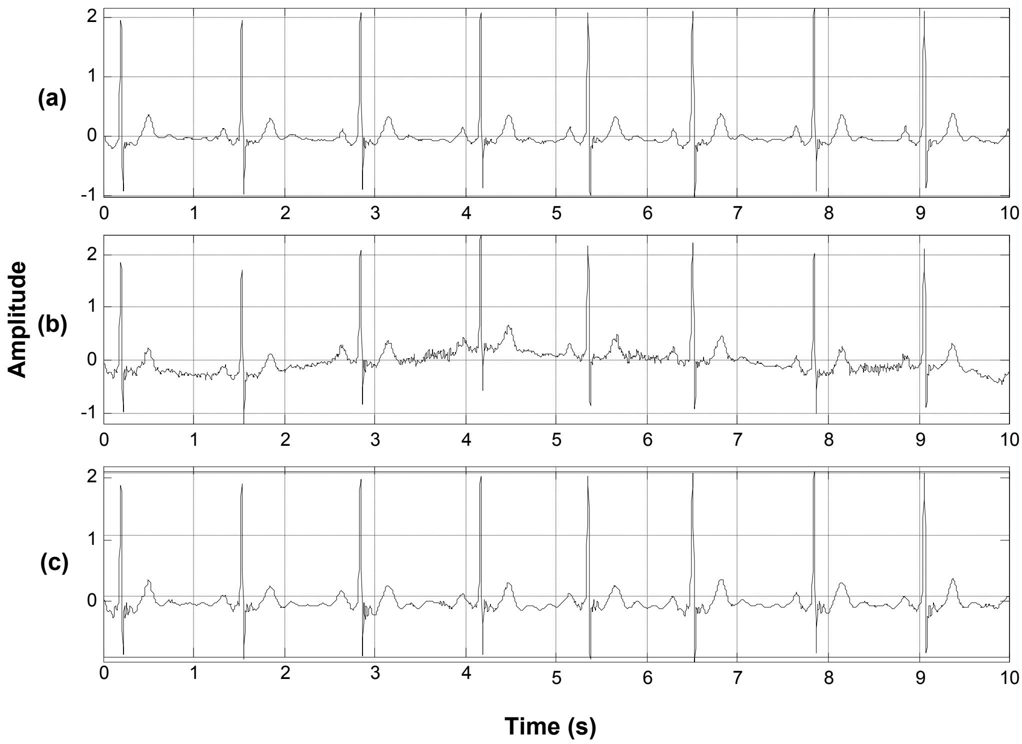

Fig. 4.6 Suppression of artifacts in ECG using SWT: (a) artifact-free ECG, (b) noisy ECG (SNR = 5 dB) and (c) ECG denoised using SWT (output SNR = 18.4 dB).

4.3 Denoising using Stationary Wavelet Transform

Stationary wavelet transform is another method designed to overcome the lack of translation-invariance of wavelet transform and pseudo-Gibbs phenomenon. The translation-invariance property was achieved by removing the down-samplers and up-samplers in the signal path of traditional discrete wavelet transform and up-sampling the wavelet filter coefficients by a factor of $2^{(i-1)}$ for i^{th} level of decomposition or reconstruction. The implementation of SWT based denoising is shown in Fig. 4.5.

The processed output ECG signal with SWT based denoising is shown in Fig. 4.6. When SWT based denoising is applied on artifact-free ECG, an output SNR of 24.5 was obtained. It can be observed that the induced distortion for SWT based denoising on artifact-free ECG signals is slightly higher than that of TIWT based denoising. For a simulated noisy ECG signal with input SNR of 5 dB, the processed output ECG resulted in an SNR of 18.44 dB. An SNR improvement of about 4.5 dB and 1.8 dB was observed when compared to DWT and TIWT based denoising. It can also be observed that the ripples introduced in the Q and S part of QRS complex was reduced by about 50 % in SWT method when compared to DWT based denoising method. A comparison of the performance of DWT, TIWT and SWT for different number of circular shifts in terms of output SNR with and without QRS complexes is given in Table 4.1 for artifact-free ECG and simulated noisy ECG. It can be seen that the performance of TIWT was higher than SWT based denoising when applied on artifact-free ECG, while the performance of SWT was found to higher for noisy ECG.

4.4 Discussion

It was observed that ripples were induced due to the effect of Gibbs phenomenon at the vicinity of sharp transitions. The translation-invariant denoising and stationary wavelet transform based noise suppression methods were investigated to suppress these denoising related distortions. To quantify the performance of the denoising methods in ripple reduction in the neighborhood of R peak, SNR and RMS error analysis was used by removing QRS complex. The performance of translation-invariant wavelet transform based denoising was found to be dependent on the number and the locations of sharp transitions in the input ECG signal. Hence, it is difficult to fix a particular value for the number of circular shifts involved in its implementation. For an n-sample signal, the time complexity of translation invariance based denoising was of the order of $n \log(n)$. Stationary wavelet transform was found to be superior to TIWT due to comparatively lower time complexity and its performance being independent of the location and number of sharp transitions. TIWT based denoising technique could be used to applications where there is lesser time and memory constraint as in the case of offline processing. But, for automatic detection systems which require online processing and SWT based denoising technique is more promising. The comparative evaluation of DWT, TIWT and SWT based denoising is presented in Chapter 5.

Chapter 5
TESTS AND RESULTS

5.1 Introduction

For evaluating the denoising technique, it was applied on ECG signals with simulated artifacts. Measures such as SNR, percentage RMS difference (PRD), L2 norm and MaxMin improvement indices are used for measure the performance and induced distortion. The effectiveness of the denoising is also validated using the improvement in R-peak detection after denoising. The evaluation is carried out using Matlab based implementation of the technique. The details of the ECG signal used for validation are described in Section 5.2. Section 5.3 describes the measures used for evaluation. The results for ECG with simulated artifacts and real artifacts are presented in Section 5.4 and 5.5, respectively.

5.2 ECG Signals Used for Validation

The denoising technique was evaluated by applying it on ECG signals with known levels of artifacts. For this purpose, signals with simulated artifacts were generated by adding artifact-free ECG and signal-free artifacts of 10 s duration. A total of 15 records (100, 101, 103, 105, 106, 116, 118, 119, 123, 202, 203, 210, 213, 220, and 232) from MIT-BIH arrhythmia database [45] with 360 Hz sampling frequency and 11-bit resolution were used. A total of 3 records (baseline wander: bw, muscle artifact (EMG): ma, and electrode motion artifact: em), from MIT-BIH stress test database [46] were used as ECG-free artifacts. All the signals and noise records were scaled to have the same RMS value. Signals were simulated with three kinds of noise: (a) EMG noise, (b) motion artifact, and (c) mixed noise. EMG noise was generated by adding 'bw' and 'ma' in 1:1 ratio. Motion artifact was generated by adding 'bw' and 'em' in 1:1 ratio. Mixed noise was generated by adding 'ma' and 'em' in 1:2 ratio.

Table 5.1 ECG databases from PhysioNet and their sampling frequencies

Database No.	ECG Database	Sampling Frequency (Hz)
1	MIT-BIH Normal Sinus Rhythm Database (nsrdb)	128
2	MIT-BIH Arrhythmia Database (mitdb)	360
3	MIT-BIH Noise Stress Test Database (nstdb)	360
4	MIT-BIH Atrial Fibrillation Database (afdb)	250
5	MIT-BIH ST Change Database (stdb)	360
6	MIT-BIH Malignant Ventricular Ectopy Database (vfdb)	250
7	T-Wave Alternans Challenge Database (twadb)	500
8	Sudden Cardiac Death Holter Database (sddb)	250

These ratios are in accordance with the occurrence of the noises in ambulatory recordings. The resultant noises were scaled to have the same RMS as that of the ECG signal. The signal with simulated noise was generated by adding noise-free signal $s(n)$ with scaled signal-free noise $d(n)$, as the following

$$x(n) = s(n) + \alpha\ d(n) \tag{5.1}$$

where α is used for the given required SNR as

$$(\mathrm{SNR})_{in} = 20\ \log\alpha \tag{5.2}$$

Three different noises for each simulated noise type (EMG, motion artifact, and mixed) were added to each artifact-free ECG signals to generate 45 noisy ECG records for a particular SNR.

In addition to applying the technique on signals with simulated artifacts for quantitative evaluation, the technique was also applied on ECG with real artifacts. Eight ECG databases available at PhysioBank [43], [52] were used for the investigation and validations of the proposed denoising techniques. The databases used and their sampling frequencies are given in Table 5.1. These databases [44]-[51] contain ECG signals with real artifacts and are acquired from normal subjects and patients with myocardial infarctions, transient ischemia, ventricular tachyarrhythmia, and other risk factors for sudden cardiac death. 320 ECG records of 20 s duration each were considered for evaluation by visual inspection.

Ambulatory ECG signals recorded using a Holter monitor (ECIL, Hyderabad, India) at 200 Hz with 8-bit resolution were also used. These recordings were acquired from five healthy volunteers in resting condition and during common ambulatory activities like hand movements, walking, and climbing stairs. The recordings were used to test the application "ECG Denoiser, v.2" described in Appendix A and also for validating the software.

5.3 Evaluation Measures

In addition to visual inspection of the denoised signal, several quantitative evaluation measures have been reported for assessing the effectiveness of denoising techniques. Some of these measures, requiring signals with simulated noise, are SNR improvement [12], [15], [17], [18], [21], [23], [28], [30], [33]–[38], RMS error [18], [22], [26], [29], [31], [33], and percentage RMS difference (PRD) [28], L2 norm and MaxMin based improvement indices [13], [34], [35], correlation coefficient [9], [18], [27], wavelet weighted PRD (WWPRD) [32], and wavelet energy-based diagnostic distortion measure (WEDD) [32]. R-peak detection efficiency with respect to manually marked detection has also been reported [26], [34], [35]. Generally, multiple measures are needed for performance estimation.

5.3.1 Visual Inspection

It is the primary assessment technique used to analyze the performance of a denoising technique on a noisy signal. It is very valuable to understand the distortion being introduced as well as the qualitative effects on characteristic points. For this method of evaluation, the availability of noise-free signal is not essential. Visual inspection of the results is highly subjective in nature and is an accurate technique. Minor distortions or amplitude changes could be overlooked due to limitation of the eye perception.

5.3.2 Signal-to-Noise Ratio (SNR) or Signal-to-Error Ratio (SER)

SNR improvement is the most commonly used quantitative measure [12], [15], [17], [18], [21], [23], [28], [30], [33]–[38]. For this measure, availability of noise-free signal $s(n)$ is necessary. SNR in the noisy input $x(n)$ is measured as

$$(\mathrm{SNR})_{\mathrm{in}} = 10 \log \left(\frac{\sum_{i=1}^{N} s^2(i)}{\sum_{i=1}^{N} \left(x(i) - s(i) \right)^2} \right) \tag{5.3}$$

Similarly, the SNR in the output $y(n)$ is measured as

$$(\mathrm{SNR})_{\mathrm{out}} = 10 \log\left(\frac{\sum_{i=1}^{N} s^2(i)}{\sum_{i=1}^{N}\left(y(i)-s(i)\right)^2}\right) \tag{5.4}$$

The SNR improvement is given as

$$(\mathrm{SNR})_{\mathrm{improvement}} = (\mathrm{SNR})_{\mathrm{in}} - (\mathrm{SNR})_{\mathrm{out}} \tag{5.5}$$

$$= 10 \log\left(\frac{\sum_{i=1}^{N}\left(y(i)-s(i)\right)^2}{\sum_{i=1}^{N}\left(x(i)-s(i)\right)^2}\right) \tag{5.6}$$

The output SNR measurement for noise-free input gives a measure of the distortion introduced by denoising technique.

5.3.3 Root Mean Square Error (RMSE) and Percentage RMS Difference (PRD)

Root mean square error is a measure of the deviation between the noise-free signal $s(n)$ and the noisy signal $x(n)$ [18], [22], [26], [29], [31], [33] and given by

$$\mathrm{RMSE} = \sqrt{\frac{1}{N}\left(\sum_{i=1}^{N}\left(x(i)-s(i)\right)^2\right)} \tag{5.7}$$

Percentage RMS difference (PRD) gives the relative RMS error [28] and is given by

$$\mathrm{PRD} = \sqrt{\frac{\sum_{i=1}^{N}\left(x(i)-s(i)\right)^2}{\sum_{i=1}^{N} s^2(i)}} \times 100 \tag{5.8}$$

It is seen that SNR and PRD measures are directly related. Reduction in PRD due to denoising gives a direct measure of the percentage of noise suppressed.

5.3.4 Correlation Coefficient (r)

Correlation coefficient r is a measure of statistical relationship or dependence between the signals [9], [18], [27]. In case of signals with simulated artifacts, the correlations of the input and output are calculated with the noise-free signals as

$$r_{in} = \frac{\sum_{i=1}^{N} \left(x(i)-\bar{x}\right)\left(s(i)-\bar{s}\right)}{\sqrt{\sum_{i=1}^{N} \left(s(i)-\bar{s}\right)^2} \sqrt{\sum_{i=1}^{N} \left(y(i)-\bar{y}\right)^2}} \tag{5.9}$$

and

$$r_{out} = \frac{\sum_{i=1}^{N} \left(y(i)-\bar{y}\right)\left(s(i)-\bar{s}\right)}{\sqrt{\sum_{i=1}^{N} \left(s(i)-\bar{s}\right)^2} \sqrt{\sum_{i=1}^{N} \left(y(i)-\bar{y}\right)^2}} \tag{5.10}$$

Increase in correlation is an indicator of noise suppression. In case of noise-free signals, the decrease in correlation is an indicator of distortion.

5.3.5 L2 Norm, MaxMin and Improvement Index (II)

L2 norm is measure of the energy of a signal, while MaxMin is the difference between the maximum and the minimum value in the signal [13], [34], [35]. The measurement of L2 Norm and MaxMin statistic is given by

$$L_2\left\{x\right\} = \sqrt{\sum_{i=1}^{N}\left(x(i)\right)^2} \tag{5.11}$$

and

$$\mathrm{MM}\left\{x\right\} = \max_{\forall n}\left[x(n)\right] - \min_{\forall n}\left[x(n)\right] \tag{5.12}$$

The improvement index for L2 norm and MaxMin is computed for signals with real artifacts by using an artifact-free segment. As the L2 norm and MaxMin capture different characteristics of the signals, an improvement index value close to one for both the indices indicates effective noise suppression, while a value less than and greater than unity indicates ineffective denoising and signal distortion, respectively.

$$\mathrm{II} = \frac{\left|\text{(Pre-denoising value)} - \text{(Post-denoising value)}\right|}{\left|\text{(Pre-denoising value)} - \text{(Artifact-free value)}\right|} \tag{5.13}$$

5.3.6 R-peak Detection Efficiency

The R-peak detection technique uses Pan-Tompkins' QRS detection algorithm [41] as an automated QRS detector and these peaks are compared with visually marked peaks. When ECG is corrupted with artifacts, the QRS detection algorithm may fail due to detect the QRS complexes or an artifact might be detected as a QRS complex. 'Success' gives the percentage of the correct detections, while 'Failure' is the percentage of QRS complexes missed. 'False' is the percentage of artifacts detected as QRS complexes. An increase in the value of success with decrease in the value of false indicates effective denoising. An increase in the value of failure indicates suppression of QRS complexes and an increase in the value of failure indicates induced distortions [26], [34], [35].

5.4 Results for ECG Signals with Simulated Artifacts

The denoising technique was evaluated for simulated noisy ECG signals with input SNR values ranging from -10 to 10 dB in steps of 5 dB. For artifact suppression, the denoising control parameters for a specific input SNR were set empirically by visual inspection of the noise content in the signal. For ECG with simulated EMG noise, the EMG denoising control parameter, ε is set to 0.6, 0.3, 0.05, 0.1 and 0.01 for input SNR of -10, -5, 0, 5 and 10 dB, respectively. The value of motion artifact denoising control parameter, η is to 0 for all SNR values due to the absence of motion artifacts in the noisy signal. For ECG with simulated motion artifacts, ε is set to 0.01 due to presence of baseline wander and high frequency noise in the noisy signal, while η is set to 0.7, 0.6, 0.5, 0.02 and 0.01 for input SNR of -10, -5, 0, 5 and 10 dB, respectively. For ECG with mixed noise, ε is set to 0.3, 0.2, 0.1, 0.05 and 0.01 with the corresponding values of η set to 0.6, 0.5, 0.5, 0.02 and 0.01, the for input SNR of -10, -5, 0, 5 and 10 dB, respectively.

The results obtained for DWT based denoising in terms of SNR improvement, reduction in PRD, L2 norm and MaxMin improvement, and correlation coefficient are given in Tables 5.2, 5.3, 5.4 and 5.5, respectively. For EMG suppression, as the input SNR increased from -10 to 10 dB, the SNR improvement was observed to decrease from 12.9 to 8.7 dB and the extent of noise suppression (in terms of reduction in PRD) was observed to increase from 63% to 78%. The L2 norm and MaxMin values close to unity for input SNR values -10 to 0 dB indicate effective denoising without signification distortion introduced in the ECG. It can be seen that the L2 norm improvement is 1.2 and 1.5 for input SNR values of 5 and 10 dB indicating that the extent of distortion induced is greater than that of artifact suppression. An improvement in correlation coefficient from 0.3 to 0.8 is observed for input SNR of -10 dB indicating effective denoising, while the correlation value increased from 0.95 to 0.99 is for input SNR of 10 dB. For motion artifact suppression, SNR improvement ranging from 14.97 to 10.8.67 dB for input SNR of -10 to 10 dB indicates efficient suppression of motion artifacts. It can also be seen from Table 5.2 that SNR improvement for input SNR of 5 dB deviates from the improvement pattern and a value of 4.02 is obtained. This is due the

Table 5.2 Mean (standard deviation) of SNR improvement in dB for simulated noisy ECG processed using DWT based denoising. Total no. of records = 45.

Noise type	Input SNR (dB)				
	-10	-5	0	5	10
EMG	12.98 (0.20)	12.71 (0.21)	12.10 (0.26)	10.89 (0.65)	8.71 (1.20)
Motion art.	14.97 (0.39)	12.38 (0.87)	8.65 (1.29)	4.02 (1.62)	8.67 (1.28)
Mixed	14.46 (0.68)	11.92 (0.98)	8.05 (1.21)	3.70 (1.53)	4.06 (0.83)

Table 5.3 Mean reduction in PRD (in %) simulated noisy ECG processed using DWT based denoising. Total no. of records = 45.

Noise type	Input SNR (dB)				
	-10	-5	0	5	10
EMG	77.57	76.83	75.14	71.39	62.99
Motion art.	82.13	75.83	62.66	36.09	62.76
Mixed	81.02	74.50	60.04	34.02	37.07

Table 5.4 Mean improvement indices of L2 norm [MaxMin] for simulated noisy ECG processed using DWT based denoising. Total no. of records = 45.

Noise type	Input SNR (dB)									
	-10		-5		0		5		10	
EMG	0.95	[0.83]	0.97	[0.81]	1.00	[0.84]	1.23	[0.86]	1.47	[0.80]
Motion art.	1.04	[0.93]	1.19	[1.02]	1.51	[1.15]	1.52	[1.15]	1.12	[0.71]
Mixed	1.07	[0.94]	1.20	[1.02]	1.55	[1.14]	2.52	[1.39]	1.83	[0.76]

Table 5.5 Mean output r [input r] for simulated noisy ECG processed using DWT based denoising. Total no. of records = 45.

Noise type	Input SNR (dB)									
	-10		-5		0		5		10	
EMG	0.80	[0.30]	0.92	[0.49]	0.97	[0.71]	0.98	[0.87]	0.99	[0.95]
Motion art.	0.83	[0.30]	0.91	[0.49]	0.94	[0.70]	0.94	[0.87]	0.99	[0.95]
Mixed	0.80	[0.30]	0.90	[0.49]	0.93	[0.70]	0.94	[0.87]	0.98	[0.95]

Table 5.6 Mean (standard deviation) of SNR improvement in dB for simulated noisy ECG processed using TIWT based denoising. Total no. of records = 45.

Noise type	Input SNR (dB)				
	-10	-5	0	5	10
EMG	14.37 (0.33)	13.93 (0.38)	13.48 (0.37)	12.40 (0.62)	10.24 (1.12)
Motion art.	16.07 (0.51)	13.48 (0.75)	9.60 (1.03)	5.06 (1.19)	10.12 (1.37)
Mixed	15.00 (0.62)	13.19 (1.00)	9.43 (1.09)	4.99 (1.21)	10.49 (1.60)

Table 5.7 Mean reduction in PRD (in %) for simulated noisy ECG processed using TIWT based denoising. Total no. of records = 45.

Noise type	Input SNR (dB)				
	-10	-5	0	5	10
EMG	80.87	79.88	78.79	75.96	68.96
Motion art.	84.26	78.74	66.68	43.70	68.40
Mixed	82.18	77.97	65.99	43.21	69.58

Table 5.8 Mean improvement indices of L2 norm [MaxMin] for simulated noisy ECG processed using TIWT based denoising. Total no. of records = 45.

Noise type	Input SNR (dB)									
	-10		-5		0		5		10	
EMG	0.98	[0.84]	0.99	[0.84]	1.03	[0.89]	1.10	[0.96]	1.22	[1.10]
Motion art.	1.06	[0.96]	1.20	[1.08]	1.51	[1.26]	2.45	[1.19]	1.25	[1.01]
Mixed	1.03	[0.91]	1.18	[1.04]	1.50	[1.21]	2.43	[1.58]	1.29	[1.01]

Table 5.9 Mean output r [input r] for simulated noisy ECG processed using TIWT based denoising. Total no. of records = 45.

Noise type	Input SNR (dB)									
	-10		-5		0		5		10	
EMG	0.83	[0.30]	0.94	[0.49]	0.98	[0.71]	0.99	[0.87]	1.00	[0.95]
Motion art.	0.87	[0.30]	0.94	[0.49]	0.96	[0.70]	0.96	[0.87]	0.99	[0.95]
Mixed	0.83	[0.30]	0.93	[0.49]	0.95	[0.70]	0.96	[0.87]	1.00	[0.95]

Table 5.10 Mean (standard deviation) of SNR improvement in dB for simulated noisy ECG processed using SWT based denoising. Total no. of records = 45.

Noise type	Input SNR (dB)				
	-10	-5	0	5	10
EMG	14.32 (0.20)	13.77 (0.23)	13.36 (0.16)	12.74 (0.45)	10.94 (0.92)
Motion art.	15.88 (2.04)	12.12 (2.53)	7.50 (2.79)	2.54 (2.85)	10.40 (1.29)
Mixed	14.66 (1.71)	11.35 (2.33)	7.03 (2.57)	2.31 (2.73)	10.57 (1.45)

Table 5.11 Mean reduction in PRD (in %) for simulated noisy ECG processed using SWT based denoising. Total no. of records = 45.

Noise type	Input SNR (dB)				
	-10	-5	0	5	10
EMG	80.77	79.50	78.52	76.90	71.46
Motion art.	83.43	74.18	55.71	21.48	69.46
Mixed	81.16	74.86	61.35	35.47	69.97

Table 5.12 Mean improvement indices of L2 norm [MaxMin] for simulated noisy ECG processed using SWT based denoising. Total no. of records = 45.

Noise type	Input SNR (dB)									
	-10		-5		0		5		10	
EMG	0.97	[0.86]	0.98	[0.84]	1.00	[0.89]	1.11	[0.99]	1.15	[1.08]
Motion art.	1.11	[1.06]	1.29	[1.21]	1.73	[1.48]	3.09	[2.10]	1.17	[0.99]
Mixed	1.12	[1.01]	1.28	[1.01]	1.70	[1.35]	3.05	[1.89]	1.18	[0.98]

Table 5.13 Mean output r [input r] for simulated noisy ECG processed using SWT based denoising. Total no. of records = 45.

Noise type	Input SNR (dB)									
	-10		-5		0		5		10	
EMG	0.83	[0.30]	0.94	[0.49]	0.98	[0.71]	0.99	[0.87]	1.00	[0.95]
Motion art.	0.84	[0.30]	0.90	[0.49]	0.91	[0.70]	0.91	[0.87]	1.00	[0.95]
Mixed	0.79	[0.30]	0.87	[0.49]	0.89	[0.70]	0.94	[0.87]	1.00	[0.95]

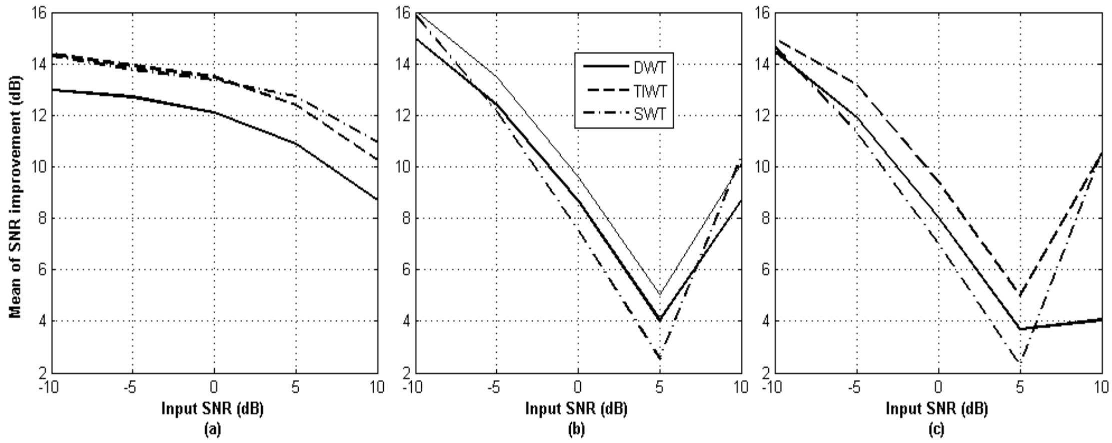

Fig. 5.1 Mean of SNR improvement versus input SNR for three noise types: (a) EMG, (b) motion artifact, and (c) mixed noise.

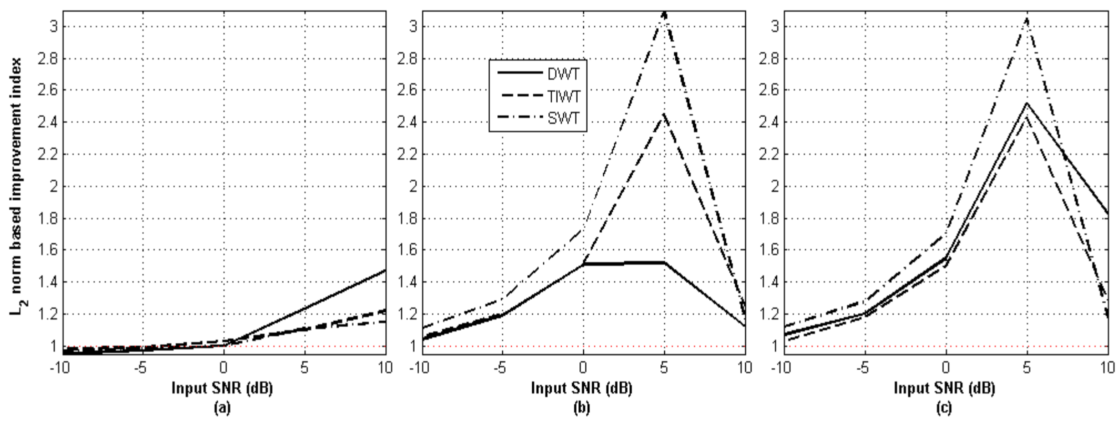

Fig. 5.2 L2 norm based improvement index versus input SNR for three noise types: (a) EMG, (b) motion artifact, and (c) mixed noise.

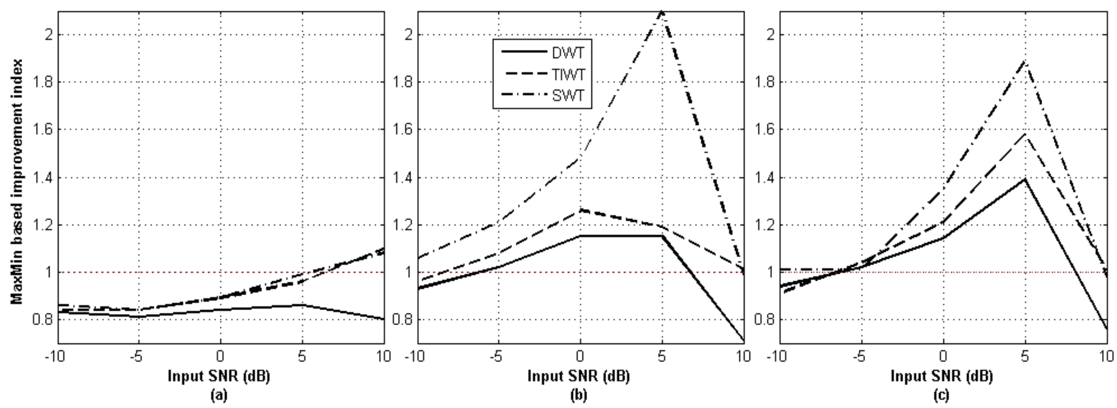

Fig. 5.3 MaxMin based improvement index versus input SNR for three noise types: (a) EMG, (b) motion artifact, and (c) mixed noise.

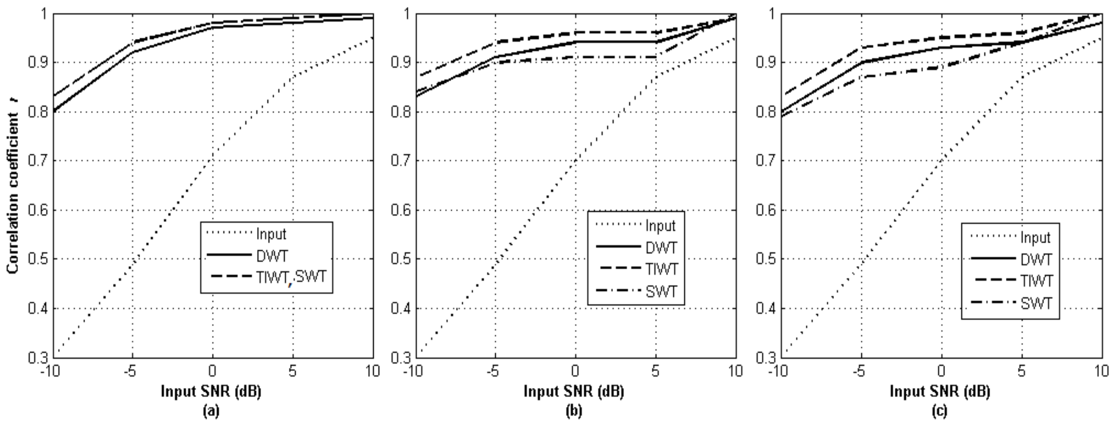

Fig. 5.4 Correlation coefficient versus input SNR for three noise types: (a) EMG, (b) motion artifact, and (c) mixed noise.

increase in large standard deviation of the artifacts resulting in lower limiting threshold values resulting to reduction in QRS amplitude. The L2 norm and MaxMin values greater than unity with the range of 1.19 to 1.52 and 1.02 to 1.15, for input SNR range of -5 to 5 dB, respectively, indicate that significant distortion is induced in the ECG. Maximum distortion was obtained for an input SNR of 5 dB. This is due to the reduction in overall mean value of the signal and its wavelet coefficients at each level, resulting in resulting reduction of the amplitude of the QRS complex. This results in higher limiting thresholds and lower induced distortion when compared to that of input SNR of 5 dB. On the contrary, the distortions induced caused by denoising for the ECG with input SNR 10 dB is lesser as the mean and variance values of the noisy signal were closer that of the artifact-free signal. For correlation coefficient, a similar trend can be seen with a value of 0.83 for -10 dB input SNR and 0.99 dB for 10 dB input SNR. The results from multiple quantitative measures indicate that EMG artifact suppression technique is efficient and better than most of the earlier reported artifact suppression techniques. The trend for suppression of mixed artifacts is seen to be similar to that of motion artifacts as the occurrence of motion artifacts is twice as high as that of EMG noise.

The results for TIWT based denoising in terms of SNR improvement, reduction in PRD, L2 norm and MaxMin improvement, and correlation coefficient are given in Tables 5.6, 5.7, 5.8 and 5.9, respectively. A similar trend can be observed for TIWT based denoising with an improved performance due to ripple suppression can be observed for suppression of EMG. For TIWT, the SNR improvement is seen to range from 10.2 to 14.4 dB which is 2 dB greater than that of DWT based denoising and percentage noise suppression is seen to range from 69% to 81 % for input SNR values from -10 to 10 dB. An improvement of 2 dB when

Table 5.14 Rate of success, failures, and false detection in percentage by the automated R-peak detection algorithm for simulated noisy ECG for different input SNR (in dB) values. Total number of cardiac cycles = 288 each.

Type of ECG	Success (%)				Failure (%)				False (%)			
	-10	-5	0	5	-10	-5	0	5	-10	-5	0	5
Noisy	94.44	94.79	99.65	100	6.25	4.86	0.35	0	21.18	6.94	1.04	0
Denoised	99.31	99.31	100	100	0.69	0.69	0.0	0	14.93	2.08	0.0	0

Table 5.15 Rate of success, failures, and false detection in percentage by the automated R-peak detection algorithm for simulated noisy ECG. Total number of cardiac cycles = 3456.

Type of ECG Record	Success (%)	Failure (%)	False (%)
Pre-denoising	97.47	2.43	7.12
Post-denoising	99.65	0.35	4.25

compared to the DWT based denoising was observed for TIWT based motion artifact suppression indicating better performance with SNR improvement ranging 14.5 to 4.1 dB. It can be seen that the L2 norm and MaxMin improvement indices are closer to unity indicating better performance. A comparatively higher output correlation coefficient is observed with a value of 1.0 for input SNR of 10 dB. A similar trend can be observed with an improved performance due to ripple suppression and reduction in the suppression of the amplitude of QRS complex can be observed for motion artifact suppression. It can be seen that the SNR improvement ranges from 16 dB to 10 dB for SNR input of -10 to 10 dB. The improvement in L2 norm and MaxMin indices indicates that the suppression of amplitude of the QRS complex is significantly reduced. Although, the motion artifact suppression is inducing some distortions, it is still very effective in removing the artifacts. This is indicated by significant improvement in the correlation coefficient values and the resultant values being close to unity. A similar trend with SNR improvement ranging from 15.0 to 10.5 dB for SNR input of -10 to 10 dB can be observed for mixed artifact suppression.

The results for SWT based denoising in terms of SNR improvement, reduction in PRD, L2 norm and MaxMin improvement, and correlation coefficient are given in Tables 5.10, 5.11, 5.12 and 5.13, respectively. For SWT based denoising, a similar performance as

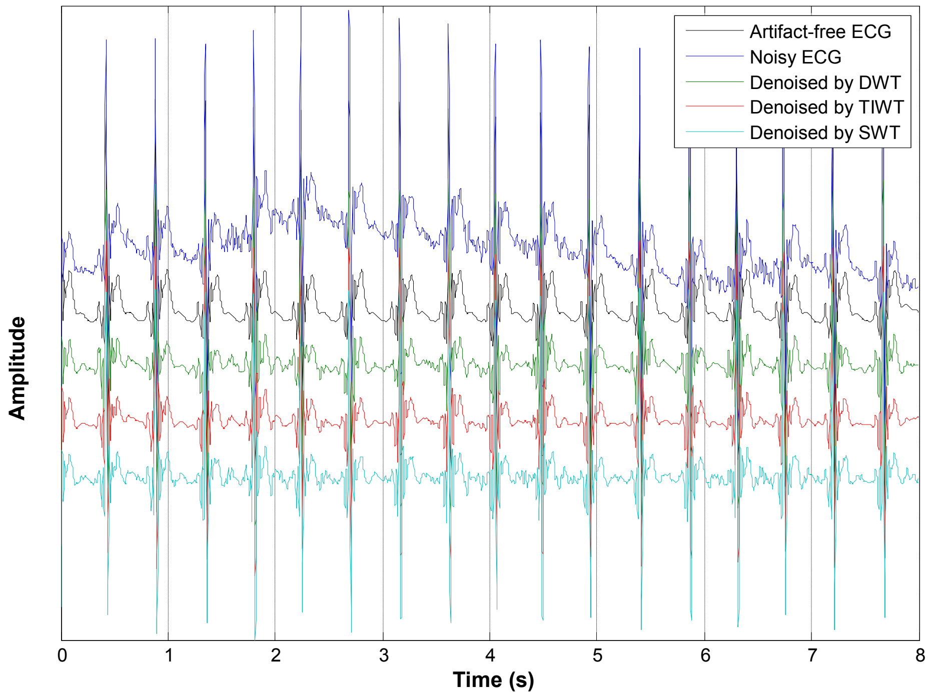

Fig. 5.5 Suppression of EMG noise in simulated noisy ECG with input SNR = -5 dB with output SNR of 7.42, 8.75 and 8.76 dB for DWT, TIWT and SWT based denoising. (ECG amplitude in arbitrary units and shifted for non-overlapping plots of the waveform.)

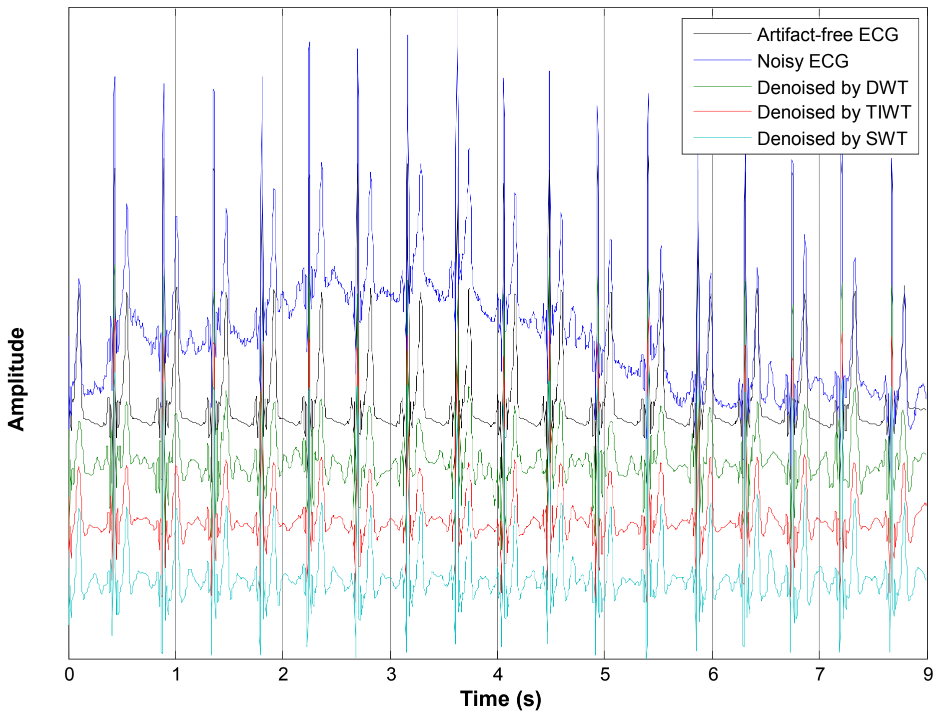

Fig. 5.6 Suppression of motion artifact in simulated noisy ECG with input SNR = 0 dB with output SNR of 6.74, 8.46 and 8.01 dB for DWT, TIWT and SWT based denoising. (ECG amplitude in arbitrary units and shifted for non-overlapping plots of the waveform.)

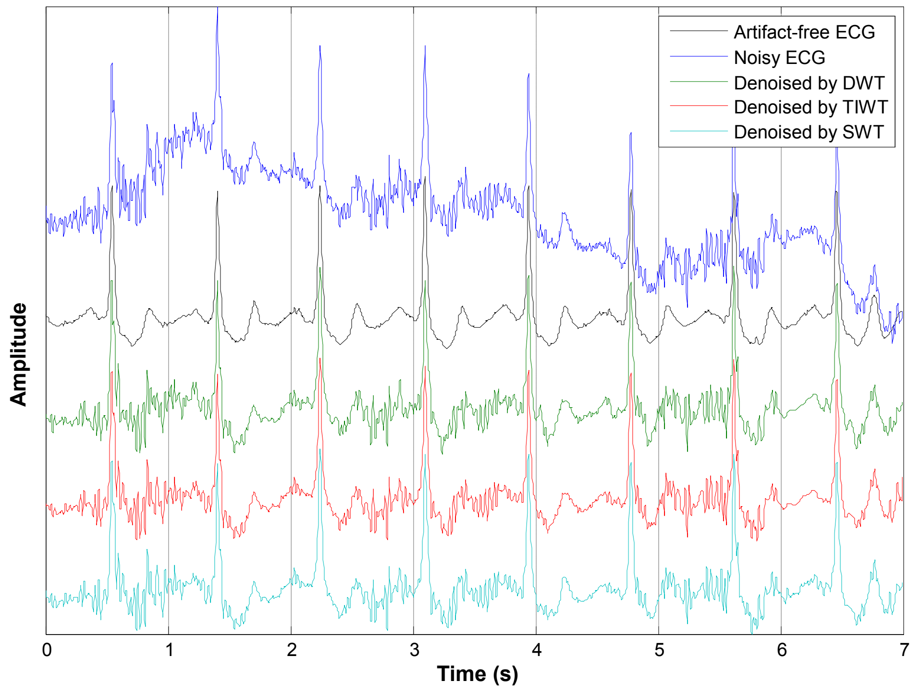

Fig. 5.7 Suppression of mixed noise in simulated noisy ECG with input SNR = 5 dB with output SNR of 11.02, 12.27 and 12.30 dB for DWT, TIWT and SWT based denoising. (ECG amplitude in arbitrary units and shifted for non-overlapping plots of the waveform.)

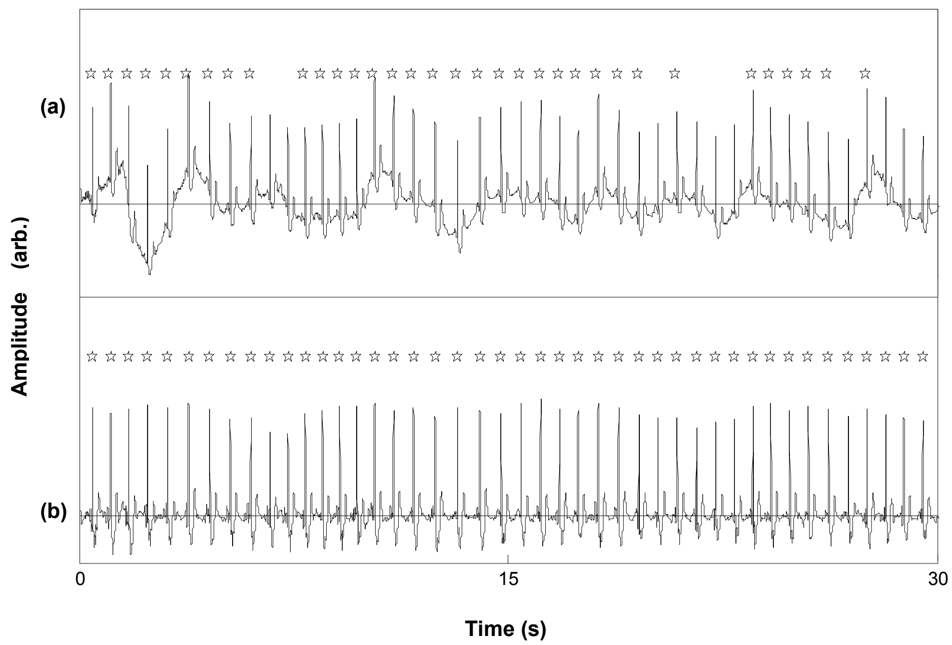

Fig. 5.8 Automated R-peak detection applied on ambulatory ECG: (a) pre-denoising and (b) post-denoising.

seen for DWT based denoising was observed for EMG artifact suppression. But the performance is worse for SWT based motion artifact suppression, indicating that it is not efficient in motion artifact reduction.

Fig. 5.1 shows that SWT and TIWT based denoising has similar performance when compared to that of DWT based denoising for ECG corrupted by EMG noise, while the performance is bit poorer for motion artifact suppression. These results are validated with L2 norm and MaxMin based improvement indices, and the improvement in correlation coefficient values as shown in Fig. 5.2, Fig. 5.3 and Fig. 5.4, respectively. Fig. 5.5, 5.6 and 5.7 show the suppression of EMG noise, motion and both in simulated noisy ECG, respectively.

The performance of R-peak detection based on Pan-Tompkins' algorithm applied on noisy ECG and denoised ECG is shown in Fig. 5.8. It can be observed that Pan-Tompkins' QRS detection algorithm, which was designed to detect QRS complexes for wide range of cardiac conditions, may fail in the presence of noise and artifacts. Table 5.14 and 5.15 shows increase efficiency of the automatic R-peak detection technique and the reduction in percentage of false peak detection due to denoising when applied on ECG signals with simulated EMG and motion artifacts. The evaluation of R-peak efficiency is carried out on DWT based denoising as the performance of DWT, TIWT and SWT are the same with respect the QRS complexes. It can be observed that as the SNR decreases the efficiency of R-peak detection was observed to be reduced, which was restored by denoising the noisy ECG signals. The performance saturates for input SNR of 5 dB with 100 % detection of the QRS complex.

5.5 Results for Ambulatory ECG with Real artifacts

It is important to inspect the performance of the denoising technique on ECG signals with abnormal cardiac activities as many of the denoising techniques which are efficient in artifact suppression for ECG signals from normal subjects fail in presence of arrhythmias. Effective artifact suppression has been observed by visual inspections for ambulatory ECG signals with atrial fibrillation as shown in Fig. 5.9 It can be seen that ripples of higher amplitude are introduced for DWT based denoising leading to lesser retention in the morphological shape. This is overcome by TIWT and SWT based denoising, where the amplitude of the ripples is lower and the morphological shapes are retained. It can also be observed that technique was efficient for a heart rate as low as 45 beats per minute. Fig 5.10 shows the performance for

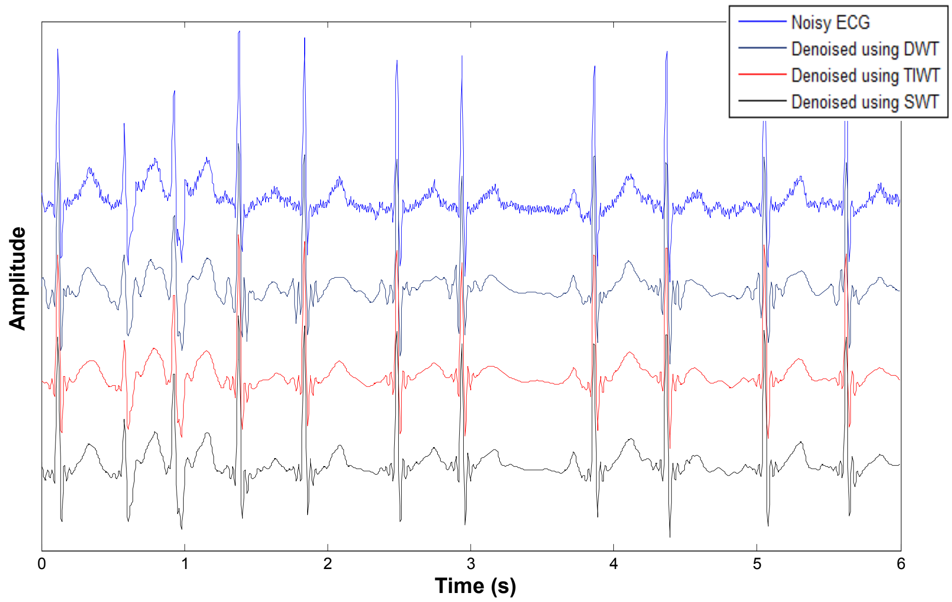

Fig. 5.9 Suppression of artifacts in patient's ambulatory ECG with atrial fibrillation. (ECG amplitude in arbitrary units and shifted for non-overlapping plots of the waveform.)

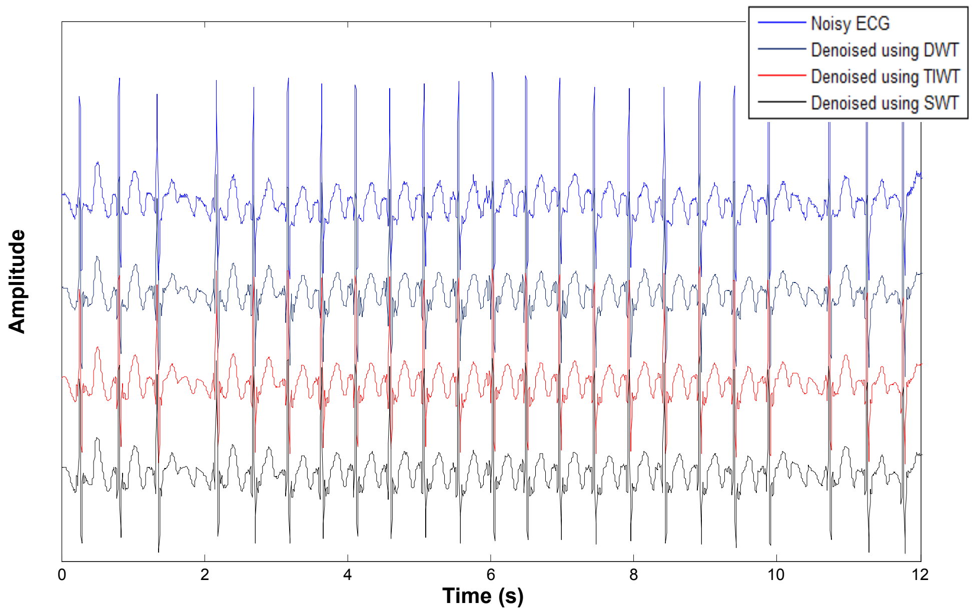

Fig. 5.10 Suppression of artifacts in patient's ambulatory ECG with atrial flutter. (ECG amplitude in arbitrary units and shifted for non-overlapping plots of the waveform.)

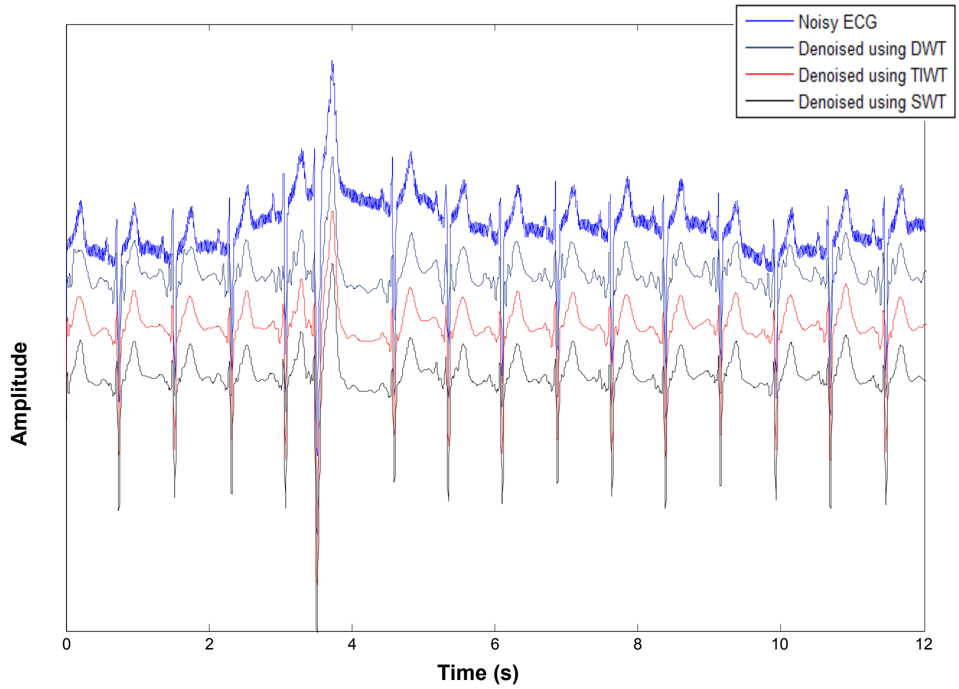

Fig. 5.11 Suppression of artifacts in patient's ambulatory ECG corrupted by noise. (ECG amplitude in arbitrary units and shifted for non-overlapping plots of the waveform.)

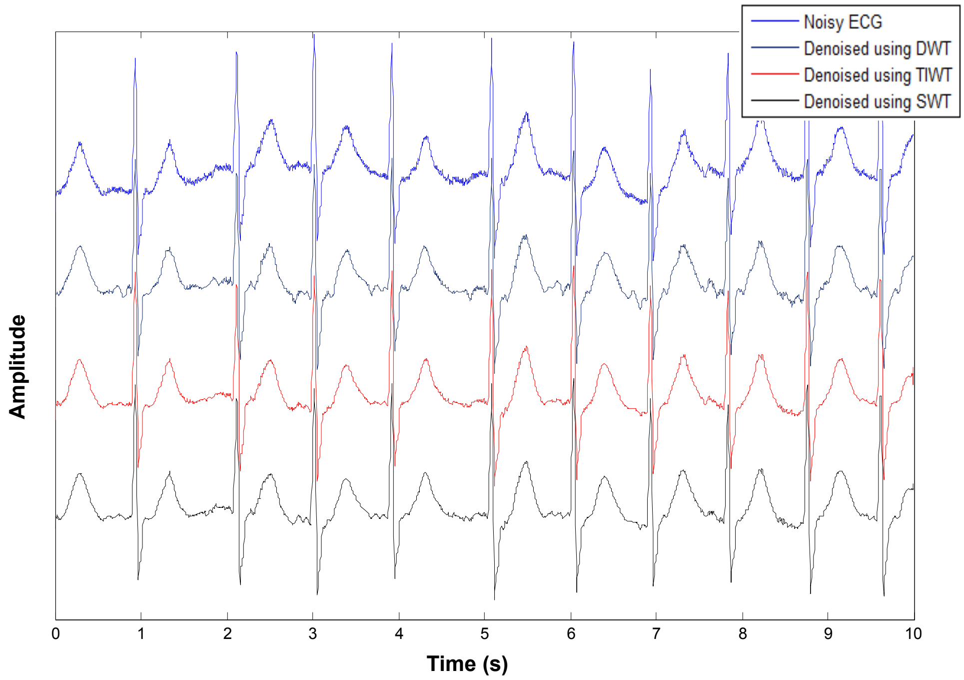

Fig. 5.12 Suppression of artifacts in patient's ambulatory ECG with ventricular bigeminy. (ECG amplitude in arbitrary units and shifted for non-overlapping plots of the waveform.)

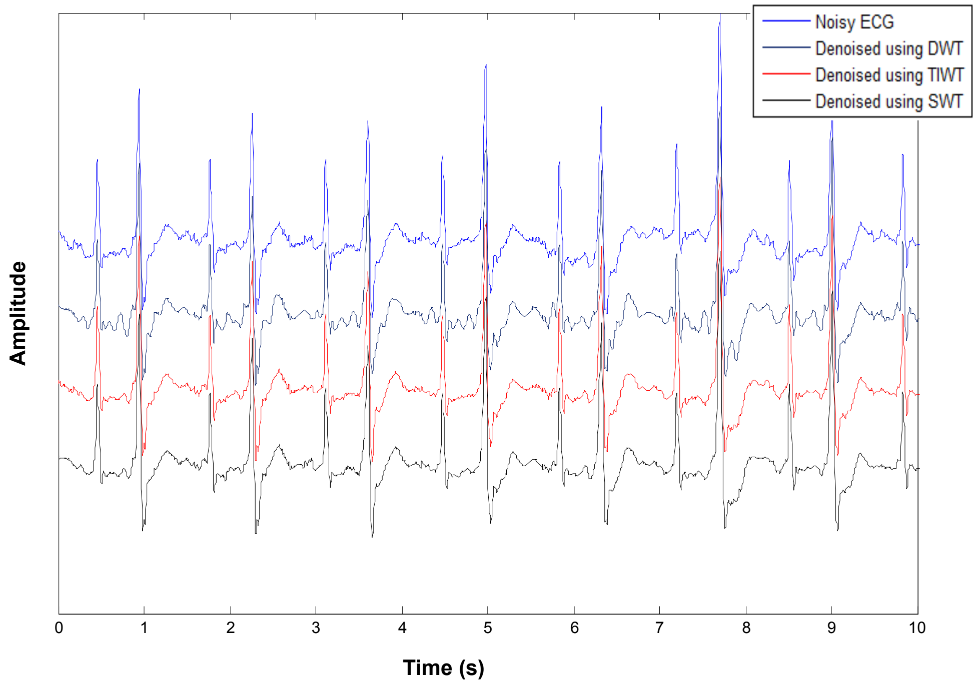

Fig. 5.13 Suppression of artifacts in patient's ambulatory ECG with pre-mature ventricular contraction. (ECG amplitude in arbitrary units and shifted for non-overlapping plots of the waveform.)

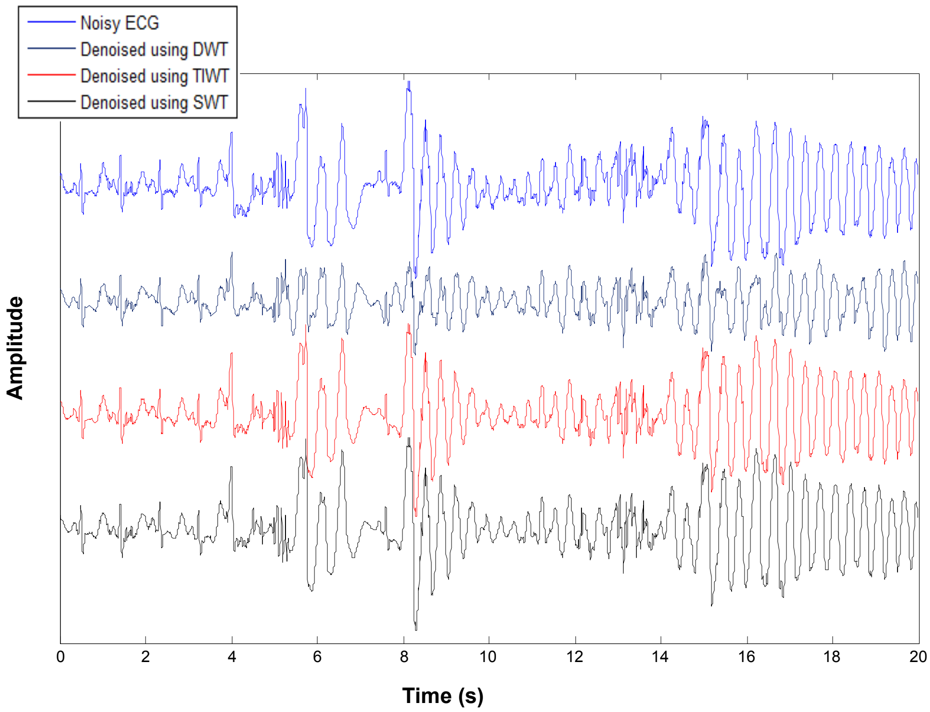

Fig. 5.14 Suppression of artifacts in patient's ambulatory ECG with ventricular fibrillation. (ECG amplitude in arbitrary units and shifted for non-overlapping plots of the waveform.)

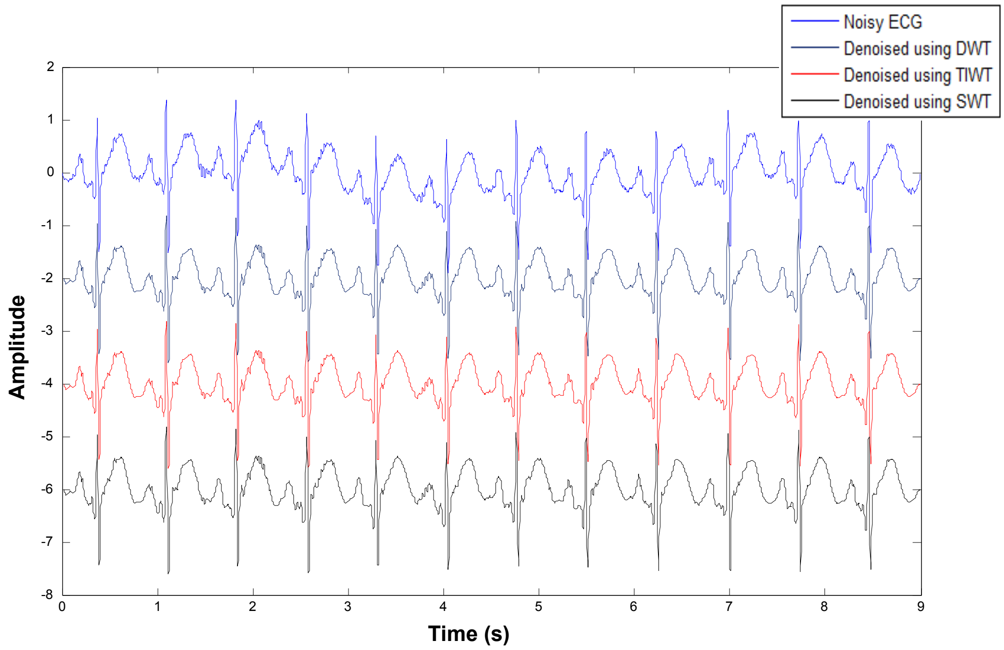

Fig. 5.15 Suppression of artifacts in patient's ambulatory ECG with ST elevation. (ECG amplitude in arbitrary units and shifted for non-overlapping plots of the waveform.)

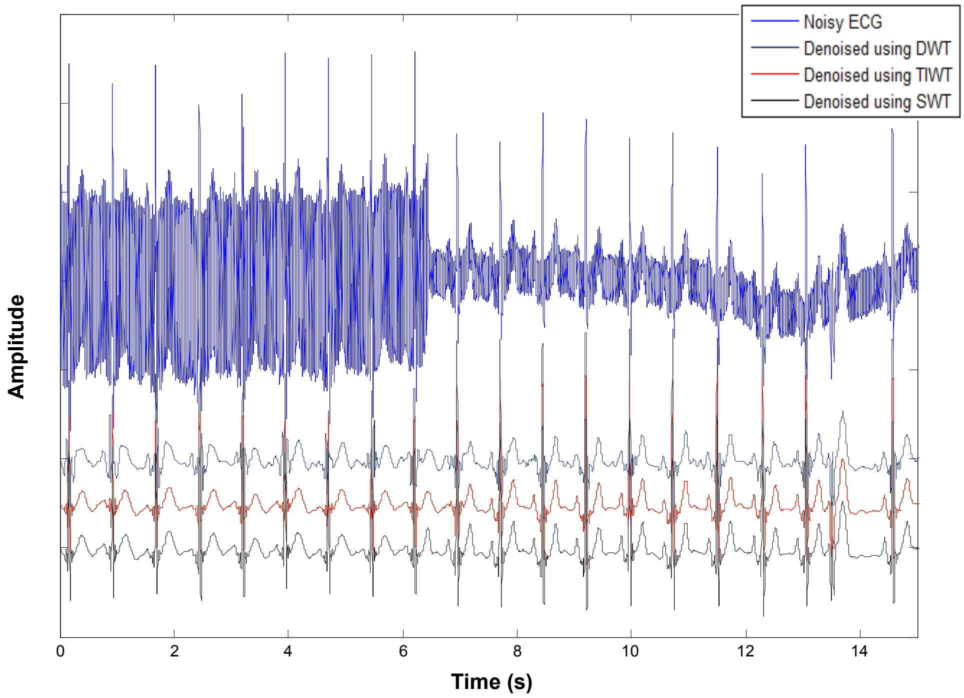

Fig. 5.16 Suppression of artifacts in patient's ambulatory ECG with its morphological features masked by high noise content. (ECG amplitude in arbitrary units and shifted for non-overlapping plots of the waveform.)

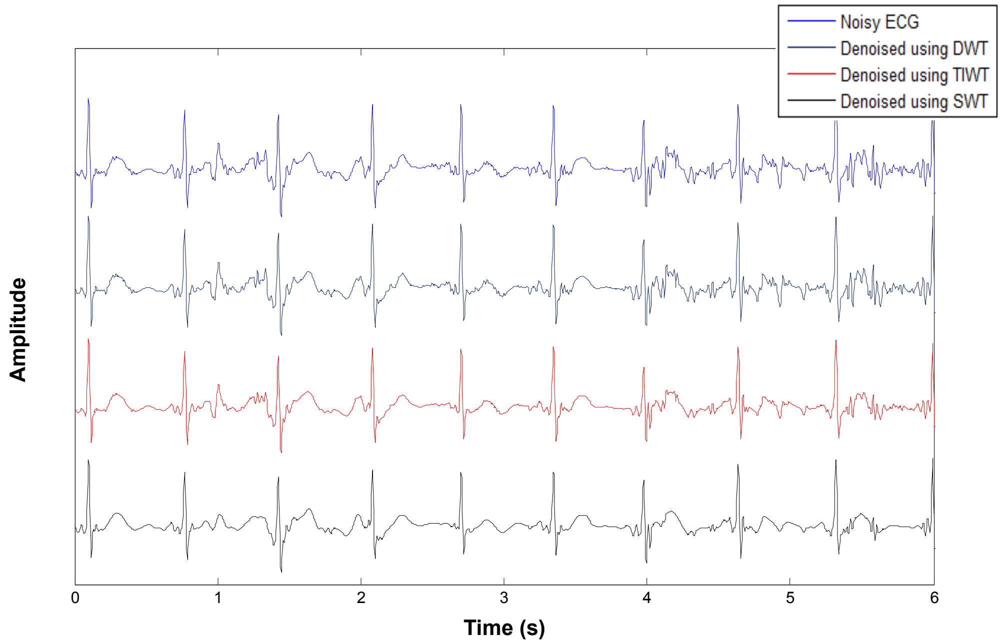

Fig. 5.17 Suppression of artifacts in ECG recorded using Holter monitor in walking condition. (ECG amplitude in arbitrary units and shifted for non-overlapping plots of the waveform.)

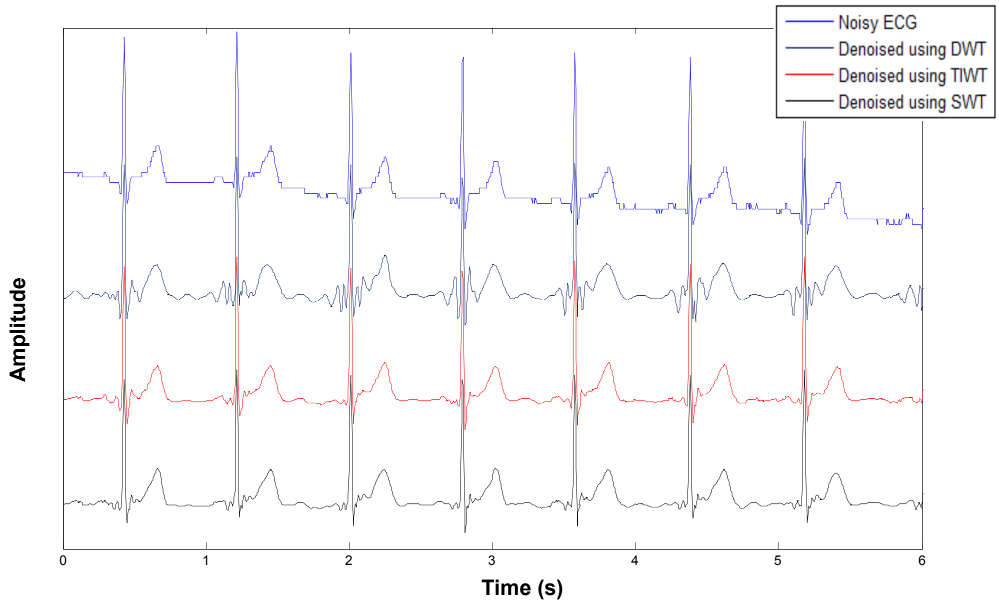

Fig. 5.18 Suppression of artifacts in ECG recorded using Holter monitor in sitting position. (ECG amplitude in arbitrary units and shifted for non-overlapping plots of the waveform.)

Table 5.16 Rate of success, failures, and false detection in percentage by the automated R-peak detection algorithm for ambulatory patient ECG. Total number of cardiac cycles = 1918.

Type of ECG record	**Success (%)**	**Failure (%)**	**False (%)**
Pre-denoising	63.19	36.81	0.10
Post-denoising	90.56	9.43	0.05

atrial flutter signals with mild EMG noise and a heart rate of 120 beats per minute. It can be observed that amount of distortions introduced due to denoising is greater than the extent of artifact suppression. Fig. 5.11 shows EMG and motion artifact suppression in ambulatory ECG. It can be seen that the P-wave is completely distorted and masked by the ripples for DWT based denoising. For TIWT, though the ripples are suppressed, the amplitude of the p-wave is suppressed in a few regions. SWT based denoising shows greater shape retention.

Fig. 5.12 shows the effect of denoising for ventricular bigeminy at a heart rate of 60 Hz. It can be seen that TIWT has the maximum shape retention while DWT based denoising has visible ripples. It can also be observed that the morphology of ventricular bigeminy is not affected by the denoising. The mild baseline wander has also been removed. The denoising technique was also found to be efficient for ECG with pre-mature ventricular contractions as shown in Fig. 5.13. When the artifact suppression algorithm was applied on ECG with ventricular fibrillation as shown in Fig. 5.14, EMG suppression technique was found to be effective. But, the motion artifact suppression technique resulted in significant reduction in the amplitude of the fibrillation. This effect is higher for DWT based suppression when compared to TIWT based suppression. Hence, motion artifact suppression technique might fail in the presence of ventricular tachycardia in the ECG signal. It can also be seen that the denoising in the regions with normal cardiac activity is not affected by the presence of arrhythmias in the denoising time frame. Fig. 5.15 shows the performance for ECG with ST elevation. The ECG signal is corrupted with baseline wander. Though there is a spectral overlap between the ST elevation or depression, it can be observed the artifact suppression has not affected the ST deviation in the ECG. But, when the motion artifact coincides with the ST elevation or depression, then motion artifact suppression technique may fail in retaining the deviation.

The performance of the denoising technique when applied for ECG signals corrupted by extreme high level noise recorded using Holter monitor is shown in Fig. 5.16. It can be observed that the denoising technique is highly efficient. Fig. 5.17 shows that SWT based denoising performed better than TIWT and DWT based denoising technique when applied on ECG signals acquired from a subject while walking using a Holter monitor, in terms of both artifact suppression and reduction in induced distortions. Fig. 5.18 shows the performance of the denoising technique on ECG signals recorded using the Holter monitor, when higher denoising control parameters were set. It can be observed that DWT based denoising introduced larger ripples, but TIWT and SWT based have not introduced any visible distortions in the denoised ECG. Also, the ST segment elevation was retained. Table 5.16 gives the success, failure and false percentages of the automatic R-peak detection algorithm for wavelet denoising when applied on ECG signals acquired using a Holter recorder available at 'Sudden cardiac death' ECG database. The result show an improvement in R-peak detection from 63.2 % to 95.6 % and a reduction in false detections from 0.1% to 0.05 %.

5.6 Summary

Artifact-free ECG signals from MIT-BIH arrhythmia database and ECG-free artifacts from MIT-BIH noise stress test database were used to generate simulated noisy ECG. SNR improvement, reduction in PRD, L2 norm and MaxMin improvements, correlation coefficient, and efficiency in R-peak detection were used for evaluating the denoising technique. Quantitative and qualitative assessment of the technique showed significant noise suppression for both EMG and motion artifacts without introducing any visible signal distortion. Better results were obtained when compared to most of the earlier reported ECG denoising techniques. For an input SNR of -10 dB, the SNR improvement of 14.7, 15.0 and 14.7 dB were obtained for DWT, TIWT and SWT based denoising, respectively. The corresponding PRD reduction values indicated 81.0 %, 82.2 % and 81.2 % of noise reduction. An improvement in QRS detection efficiency from 94.4 % to 99.3 % with reduction in false detection percentage from 21.2 % to 14.9 % was obtained for simulated noisy ECG.

Validation on ECG signals from MIT-BIH ECG databases, sudden cardiac death database and on ambulatory signals recorded using a Holter monitor showed that the technique was efficient in artifact suppression without significant distortions for normal ECG, ECG with arrhythmias, ST deviation, atrial fibrillation, atrial flutter, bigeminy, ventricular tachycardia, ventricular flutter, ventricular fibrillation and premature ventricular contraction with low and moderate noise levels. But it failed in some cases with extremely high noise. Significant improvement in QRS detection efficiency from 63.2 % to 90.6 % with reduction in false detection percentage from 0.10 % to 0.05 % was obtained for denoising of ambulatory patient ECG with various cardiac conditions.

EMG suppression technique was found to be very effective and performance was observed to be better than motion artifact suppression. The amplitude of the QRS complexes present in the artifact-free segments was found to be reduced when motion artifact is present only for a short duration in the noisy ECG. DWT based motion artifact suppression fails when ventricular fibrillation is present in the ECG and significant amount of fibrillation is suppressed. When motion artifact was superimposed on ST elevation or depression of the ECG, the deviation was suppressed in a few cases. SWT based motion artifact suppression was not as effective as the TIWT based suppression.

This page is intentionally left blank

Chapter 6
SUMMARY AND CONCLUSION

ECG signals are vital cardiac signals for analyzing the functioning of the heart. As many of the cardiac abnormalities are manifested in ECG only while performing normal day-to-day activities and during stress test, it is inevitable to record ECG corrupted by artifacts and noise. Suppression of artifacts is very important because their presence masks the morphological features and makes it difficult to get correct diagnostic information. Wavelet based denoising techniques, using discrete Meyer (dmey) wavelet, were investigated to suppress noise and artifacts in ECG. Approximate decomposition levels required for different sampling frequencies were also investigated. Level-dependent thresholding was used for EMG noise suppression with thresholds estimated from scales which predominantly represented EMG noise. Coefficient limiting was used for suppression of motion artifacts with limiting thresholds estimated from noise statistics at each scale. As ripples were introduced in the denoised ECG signals when processed using DWT, TIWT and SWT based denoising methods were investigated and implemented.

Artifact-free ECG signals from MIT-BIH arrhythmia database were used for the evaluation of the artifact suppression. The methods were validated using SNR improvement, L2 norm and MaxMin improvements, correlation coefficient, reduction in PRD and efficiency in R-peak detection. Quantitative and qualitative assessment of the technique by applying it on recordings from several healthy subjects showed that both types of artifacts were suppressed without introducing any visible signal distortion. For an input SNR of -10 dB, the SNR improvement of 14.5, 15.0 and 14.7 dB were obtained for DWT, TIWT and SWT based denoising, respectively. The corresponding PRD reduction values indicated 81.0 %, 82.2 % and 81.2 % of noise reduction. An improvement in QRS detection efficiency from 94.4 % to 99.31 % with reduction in false detection percentage from 21.2 % to 14.9 % was obtained. TIWT and SWT based denoising were found to be better than DWT based ECG denoising.

The proposed denoising techniques were also validated on ECG signals from MIT-BIH ECG databases, sudden cardiac death database and on ambulatory signals recorded using the Holter monitor. Artifact suppression was efficient in artifact suppression without significant distortions for normal ECG, ECG with arrhythmias, ST deviation, atrial fibrillation, atrial flutter, bigeminy, ventricular tachycardia, ventricular flutter, ventricular fibrillation and premature ventricular contraction with low and moderate noise levels. But, the technique was found to fail when extremely high noise levels with motion artifacts are superimposed on the ECG. Significant improvement in QRS detection efficiency from 63.2 % to 90.6 % with reduction in false detection percentage from 0.1 % to 0.05 % was obtained for denoising of ambulatory patient ECG with the abnormal cardiac conditions.

A software application based on DWT based ECG denoising has been developed for artifact suppression in 3-lead ECG signals recorded using a Holter monitor at a sampling frequency of 200 Hz.

Application of motion artifact suppression technique resulted in decrease in the amplitude of some of the QRS complexes in the artifact-free segments. Hence, there is a need for further improving the motion artifact suppression. DWT based motion artifact suppression fails when ventricular fibrillation is present in the ECG. When motion artifact gets superimposed on ST elevation or depression, the deviation may be suppressed in a few cases. A few distortions were seen in the processed ECG due to limiting function involved in the motion artifact suppression technique which resulted in a lower SNR improvement for ECG corrupted with motion artifacts when compared to ECG corrupted with EMG noise. The developed wavelet based denoising technique uses empirically set denoising control parameters. Further improvisation is possible by investigating the relation between the noise level in ECG and the denoising control parameters for an automatic selection of denoising control parameters.

Appendix A
User Manual for "ECG Denoiser, v.2"

A.1 Introduction

The "ECG Denoiser, v.2" is a graphical user interface (GUI) application developed using LabWindows Version 9.1 for denoising three-lead ECG signals acquired using a Holter monitor. It reads the ECG data from text files in Holter monitor's file format (as given in A.10) and saves the denoised data back in the same format. It graphically displays the three ECG leads simultaneously, and it has ten control buttons for the display and denoising operations: load, block, start, span, display, settings, save, print, strip chart, and background.

A.2 'Load': Input File Selection

It is used, with the help of a file-select-popup, to select the ECG file to be displayed and denoised. If the file format is correct, the three ECG lead signals are displayed, assuming the sampling frequency to be 200 Hz and with default time axis as 0-10 s. The file name and the patient ID (from the file) are also displayed.

A.3 'Block Position', 'Start', and 'Span': Segment Selection

The input data file may contain signal recording of a very long duration. For processing, the signal from the input data file is read as a block of 100 s duration. The 'Block Position (s)' is initially set as 0 s and it can be varied to navigate through the recording. The 'Start' and 'Span' can be used to navigate within the selected block. 'Start (s)' controls the start time of the displayed segment and 'Span (s)' sets its span. They can be changed by entering the time in the text box or by incrementing/decrementing the value using the up/down arrows next to the text box. When the selected segment is changed by changing either the start or the span, the displayed unprocessed segment of the signal is updated and processed for suppression of the artifacts. The presence of emergency event marker in the input data is shown as a horizontal bar above the corresponding segment of the displayed waveform.

A.4 'Display': Display Mode Selection

The ECG signals can be displayed using one of the three display modes: (a) original ECG, (b) denoised ECG, and (c) original and denoised ECG. The mode can be selected using the drop-down 'Display' option. An example of the displays using the three modes is shown in Fig. A.4.

A.5 'Settings': Selection of Processing Parameters

It is used for selecting, for each of the three leads, the processing parameters: EMG noise level, MA (motion artifact) level, and segment thresholding. Selection of the processing parameters for a specific signal segment helps in denoising optimization without introducing signal distortion. 'Denoise' button is used for denoising with the newly set parameters.

'EMG (0-1)' may be used to control the extent of suppression of EMG noise. It may be varied over 0−1, with a default value of 0. The extent of noise suppression increases as the value is increased, but too high a value may introduce distortion in the denoised ECG. A low value should be used if the segment is not contaminated by EMG noise.

'MA (0-1)' is used to control the suppression of motion artifact. Its default value is 0.5. The threshold levels for the motion artifact reduction are obtained either from the displayed segment or from a motion-artifact-free segment, as controlled by the 'Seg-Th' checkbox. If the box is not checked, the thresholds are estimated from the noisy ECG segment itself. The box can be checked for estimating the thresholds from a manually selected noise-free ECG segment. This method is expected to give better results.

Checking of the "Seg-Th" box operates as a toggle. Clicking on the unchecked box results in a new pop-up window, showing a plot of the input ECG waveform. By panning the waveform using 'Ctrl + Shift + mouse cursor', a segment which does not contain significant motion artifact can be selected. The window disappears after the 'Ok' button (below the graph after selecting the segment) is clicked, and the 'Seg-Th' box appears as checked. The threshold levels for motion artifact reduction are obtained from the selected artifact-free ECG segment. Another artifact-free segment for threshold selection can be chosen by un-checking 'Seg-Th' and clicking it again.

When the 'Denoise' button is clicked, the analysis segment is denoised using the updated parameters. Clicking the 'Cancel' button cancels the changes made and the parameter values are reverted to the previous setting.

A.6 'Save': Saving the Signal

If the display mode is 'original', the unprocessed ECG is saved. If the display mode is 'denoised' or 'original and denoised', the denoised signal is saved. There are four 'Save' modes: save complete ECG, save displayed ECG, append displayed ECG, and save screen. When one of the options is clicked, a file select pop-up appears, the directory and file name can be given. In 'save complete ECG' mode, the selected block of ECG (the three leads) are saved. In 'save displayed ECG' mode, only the selected segment is saved. In 'append displayed ECG' mode, the selected segment is appended to the data in an existing file. In 'save screen' mode, an image of the screen is saved as a file in 'png' format, for later use in a document or for printing.

A.7 Print

It can be used for printing the displayed screen. On clicking the 'Print' button, a dialog box opens for selecting the printer and setting its properties. By selecting a "PDF" printer, the displayed screen can be saved to a file

A.8 Strip Chart

It may be used for a continuous display of the three-lead ECG from the selected input file. The display mode and the processing parameters can be changed, but the save option is disabled.

A.9 'Background': Changing the Background Colour

It may be used for setting the background colour of the plots. 'Dark' mode gives a high contrast with the waveforms plotted as green (denoised) and yellow (unprocessed) colours on black background. 'Light' mode uses white background with the waveforms plotted as black (denoised) and blue (unprocessed) and it is better suited for printing the screen image.

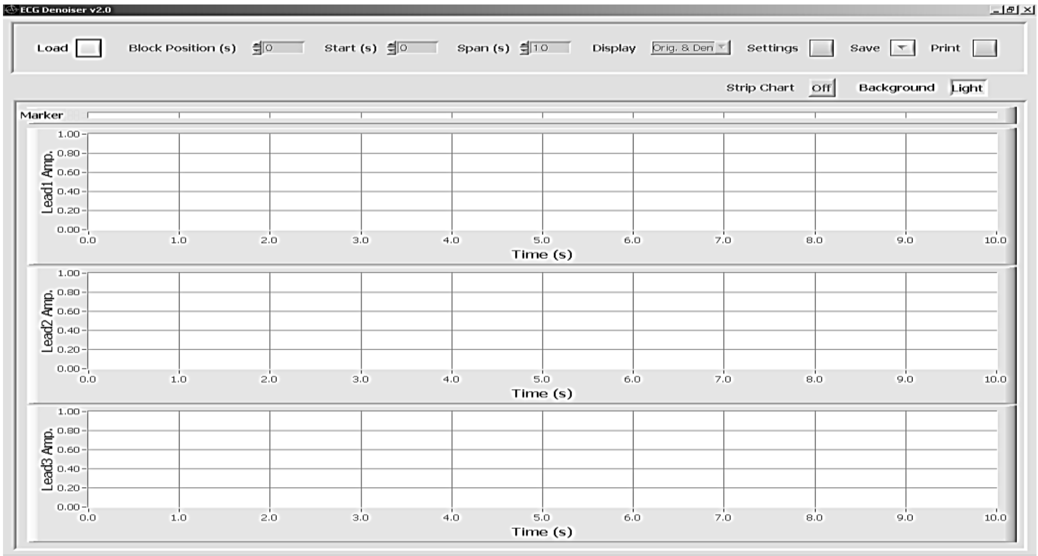

Fig. A.1 Initial view of ECG Denoiser after startup, showing the control buttons at the top.

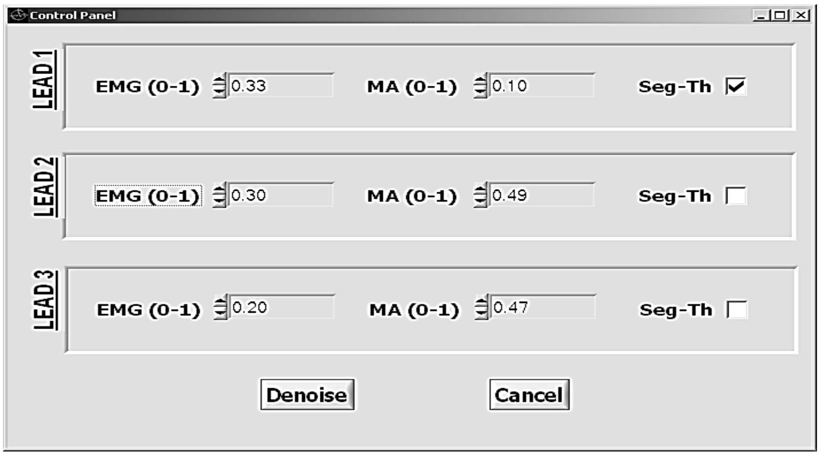

Fig. A.2 Settings panel of ECG Denoiser showing 'EMG (0-1)', 'MA (0-1)' and 'Seg-Th' fields for each lead.

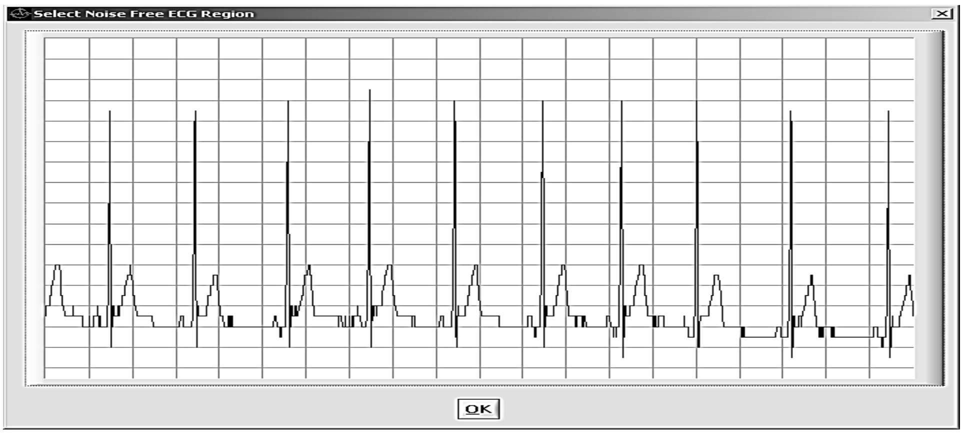

Fig. A.3 Pop-up panel for selecting motion-artifact-free segment used for calculating the threshold levels used by motion artifact reduction technique.

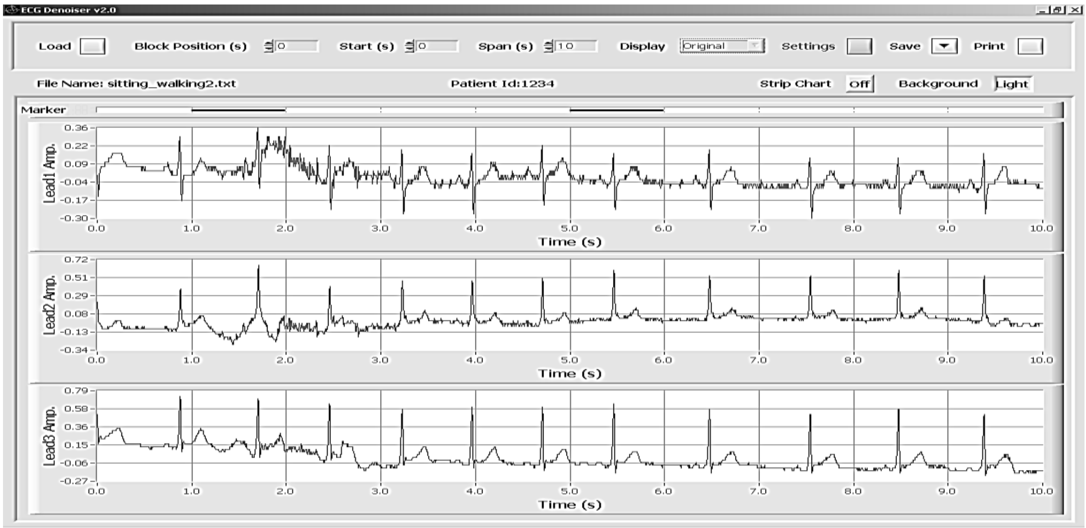

(a)

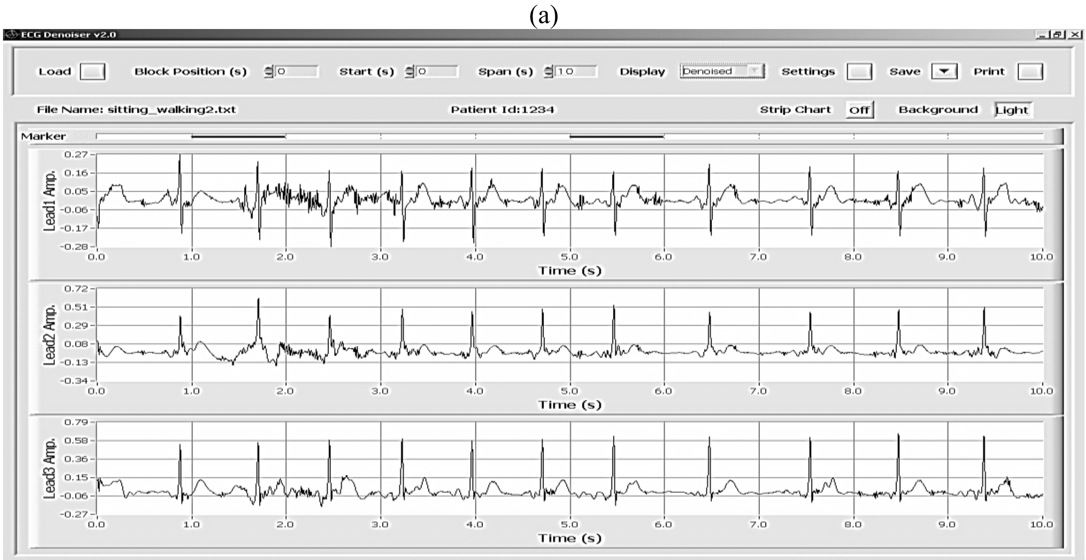

(b)

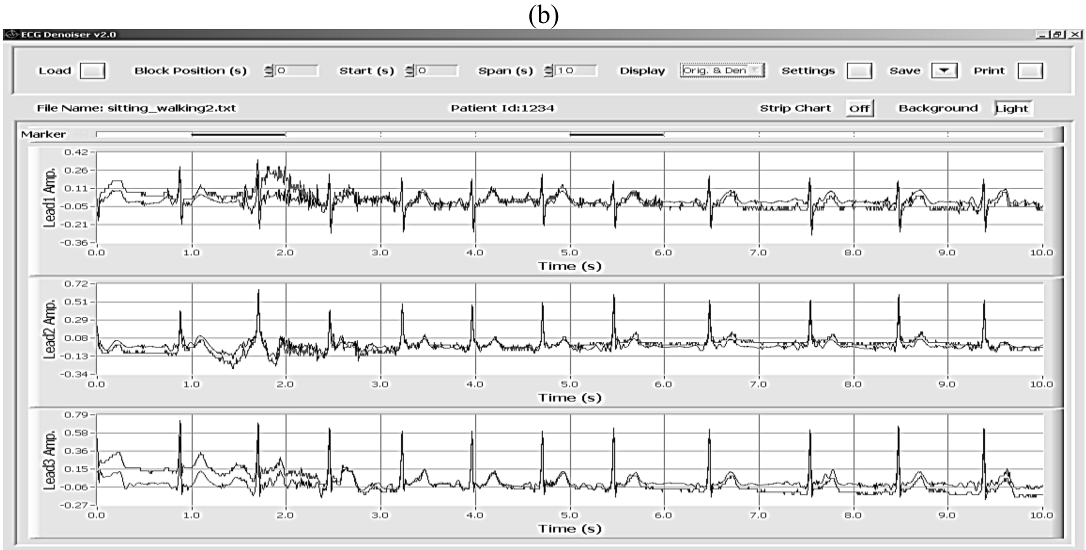

(c)

Fig. A.4 Different modes of display of ECG Denoiser: (a) Original ECG, (b) Denoised ECG, and (c) Overlapped of original and denoised ECG.

2.10 Holter Monitor File Format

The Holter monitor stores the 3-channel ECG data in text files, with extension ".txt". The instrument has an "emergency switch" which can be pressed during signal recording to indicate certain events and the status of this switch is recorded along with the signal. In the file, the first line records patient ID. Each of the subsequent lines gives a time stamp followed by the sample values for successive segment, each of 1 s duration. Each line ends with line feed <LF> and carriage return <CR>. The three channels are as the following. Channel-1: Lead-I, Channel-2: Lead-II, Channel-3: Lead-V5. Each channel is sampled at 200 Hz, and thus there are 600 sample values in each segment.

The patient ID is recorded in the first line as 'Patient Id:' (11 characters) followed by a four digit number (between 1000 to 9999, giving the patient ID). Each of the subsequent lines starts with a time stamp giving the starting time as "hh:mm:ss:" (9 characters) followed by a character giving the status of the emergency switch at that time. If the switch is pressed, the character is **'@'** else it is **'!'.** The following characters (ASCII values in the range 33-255) give the sample values for 1 s segment of the signal. The values of the three channels at each sampling instant are given as consecutive bytes corresponding to the first, second, and third channels. The format is also described in Table A.1.

Table A.1 Holter Monitor File Format

<table>
<tr><th>Line No.</th><th>Char. No.</th><th>Content</th><th>Remarks</th></tr>
<tr><td rowspan="17">1</td><td>1</td><td>Character ‘P’</td><td rowspan="11">Patient ID</td></tr>
<tr><td>2</td><td>Character ‘a’</td></tr>
<tr><td>3</td><td>Character ‘t’</td></tr>
<tr><td>4</td><td>Character ‘i’</td></tr>
<tr><td>5</td><td>Character ‘e’</td></tr>
<tr><td>6</td><td>Character ‘n’</td></tr>
<tr><td>7</td><td>Character ‘t’</td></tr>
<tr><td>8</td><td>Space</td></tr>
<tr><td>9</td><td>Character ‘I’</td></tr>
<tr><td>10</td><td>Character ‘d’</td></tr>
<tr><td>11</td><td>Character ‘:’</td></tr>
<tr><td>12</td><td>1^{st} digit of 4 digit number</td><td rowspan="4">Any 4 digit number between 1000 to 9999, giving patient ID</td></tr>
<tr><td>13</td><td>2^{nd} digit of 4 digit Number</td></tr>
<tr><td>14</td><td>3^{rd} digit of 4 digit Number</td></tr>
<tr><td>15</td><td>4th digit of 4 digit Number</td></tr>
<tr><td>16</td><td><CR></td><td rowspan="2">Separator</td></tr>
<tr><td>17</td><td><LF></td></tr>
<tr><td rowspan="21">1+ n

(n = time in s)</td><td>1, 2</td><td>‘hh’ (two digits for hours of time)</td><td>2 characters</td></tr>
<tr><td>3</td><td>Character ‘:’</td><td>Separator</td></tr>
<tr><td>4, 5</td><td>‘mm’ (two digits for minutes of time)</td><td>2 characters</td></tr>
<tr><td>6</td><td>Character ‘:’</td><td>Separator</td></tr>
<tr><td>7, 8</td><td>‘ss’ (two digits of seconds of time)</td><td>2 characters</td></tr>
<tr><td>9</td><td>Character ‘:’</td><td>Separator</td></tr>
<tr><td>10</td><td>Character ‘!’ or ‘@’</td><td>‘!’ if emergency switch off, @ if emergency switch on</td></tr>
<tr><td>11</td><td>1^{st} sample of channel-1</td><td rowspan="3">1^{st} sampling instant of n^{th} second</td></tr>
<tr><td>12</td><td>1^{st} sample of channel-2</td></tr>
<tr><td>13</td><td>1^{st} sample of channel-3</td></tr>
<tr><td>14</td><td>2^{nd} sample of channel-1</td><td rowspan="3">2^{nd} sampling instant of n^{th} second</td></tr>
<tr><td>15</td><td>2^{nd} sample of channel-2</td></tr>
<tr><td>16</td><td>2^{nd} sample of channel-3</td></tr>
<tr><td>|</td><td>|</td><td>|</td></tr>
<tr><td>|</td><td>|</td><td>|</td></tr>
<tr><td>608</td><td>200^{th} sample of channel-1</td><td rowspan="3">600^{th} sampling instant of n^{th} second</td></tr>
<tr><td>609</td><td>200^{th} sample of channel-2</td></tr>
<tr><td>610</td><td>200^{th} sample of channel-3</td></tr>
<tr><td>611</td><td><CR></td><td rowspan="2">Separator</td></tr>
<tr><td>612</td><td><LF></td></tr>
</table>

REFERENCES

[1] W. J. Tompkins, *Biomedical Digital Signal Processing: C Language Examples and Laboratory Experiments for the IBM PC*. Englewood Cliffs, NJ: Prentice Hall, 1993.

[2] A. C. Guyton and J. E. Hall, *Textbook of Medical Physiology*. 11th ed. Philadelphia, Pennsylvania: Elsevier Saunders, 2006.

[3] J. J. Carr and J. M. Brown, *Introduction to Biomedical Equipment Technology*. 4th ed. Englewood Cliffs, New Jersey: Prentice Hall, 2001.

[4] R. M. Rangayyan, *Biomedical Signal Analysis: A Case-Study Approach*. 1st ed. New York: Wiley, 2002.

[5] S. Chaudhuri, T. D. Pawar, and S. Duttagupta, *Ambulation Analysis in Wearable ECG*. New York: Springer, 2009.

[6] G. C. Agarwal and G. L. Gottlieb, "An analysis of the electromyogram by Fourier, simulation and experimental techniques," *IEEE Trans. Biomed. Eng.*, vol. 22, no. 3, pp. 225–229, 1975.

[7] A. V. Alste and T. S. Schilder, "Removal of base-line wander and power-line interference from ECG by efficient FIR filter with a reduced number of taps," *IEEE Trans. Biomed. Eng.*, vol. 32, no. 12, pp. 1052–1060, 1985.

[8] H. Lee and Z. Bien, "Variable bandwidth filter for reconstruction of bio-medical signals with time-varying instantaneous bandwidth," in *Proc. 24th Joint Conf. IEEE EMBS/BMES*, Texas, 2002, pp. 141–142.

[9] M. Dai and S. L. Lain, "Removal of baseline wander form dynamic electrocardiogram signals," in *Proc. 2nd Int. Congr. Image and Signal Processing*, Tianjin, China, 2009, pp. 1–4.

[10] V. S. Chouhan and S. S. Mehta, "Total baseline removal of baseline drift from ECG signal," in *Proc. Int. Conf. IEEE Computing: Theory and Applications*, Kolkata, India, 2007, pp. 512–515.

[11] H. Sadabadia, M. Ghasemi, and A. Ghaffari, "A mathematical algorithm for ECG denoising using window analysis," *Biomed Pap Med Fac Univ Palacky Olomouc Czech Repub J.*, vol. 151, pp.73–78, 2007.

[12] M. Z. U. Rahman, R. A. Shaik, and D. V. R. K. Reddy, "An efficient noise calculations technique to remove noise from the ECG using normalized signal regressor LMS

algorithm," in *Proc. Int. Conf. IEEE Bioinformatics and Biomedicine*, Washington, D. C. , 2009, pp. 257–260.

[13] D. A. Tong, K. A. Bartels, and K.S. Honeyager, "Adaptive reduction of motion artifacts in ECG," in *Proc. 2nd Joint Conf. IEEE EMBS/BMES*, Houston, Texas, 2002, pp. 1403−1404.

[14] D. Jeong and S. Kim, "Development of a technique for cancelling motion artifact in ambulatory ECG monitoring system," in *Proc. Int. Conf. Convergence and Hybrid Information Technology*, Busan, Korea, 2008, vol. 3, pp. 954–961.

[15] O. Sayadi and M. B. Shamsollahi, "ECG denoising and compression using modified extended kalman filter structure," *IEEE Trans. Biomed. Eng.*, vol. 55, no. 9, pp. 2240−2248, 2008.

[16] N. T. Thakor and Y. S. Zhu, "Applications of adaptive filtering to ECG analysis: noise cancellation and arrhythmia detection," *IEEE Trans. Biomed. Eng.*, vol. 38, no.8, pp. 785−794, 1991.

[17] R. Sameni, M. B. Shamsollahi, C. Jutten, and G. D. Clifford, "A nonlinear Bayesian filtering framework for ECG denoising," *IEEE Trans. Biomed. Eng.*, vol. 54, no.12, pp. 2171−2185, 2007.

[18] Y. Wu, R. M. Rangayyan, and N. Sin-Chun, "Cancellation of artifacts in ECG signals using a normalized adaptive neural filter," in *Proc. 29th Annu. Int. Conf. IEEE Engineering in Medicine and Biology Society*, Lyon, France, 2007, pp. 23−26.

[19] A. K. Barros, A. Mansour, and N. Ohnisi, "Removing artifacts from ECG signals using independent component analysis," *Neurocomputing J.*, vol. 22, pp. 173−186, 1998.

[20] F. L. Foresta, N. Mammone, and F. C. Morabito "Artifact cancellation from electrocardiogram by mixed wavelet-ICA filter," in *Proc. WIRN/NAIS 2005 Workshop*, 2006, pp. 78–82.

[21] M. B. Velasco, B. Weng, and K. E. Barner, "ECG denoising and baseline wander correction based on empirical mode decomposition," *Comput. Biol. Med.*, vol. 38, pp. 1−13, 2008.

[22] N. Li and P. Li, "An improved algorithm based on EMD-wavelet for ECG denoising," in *Proc. 2009 Int. Joint Conf. Computational Sciences and Optimization*, Hainan, China, 2009, pp. 825−827.

[23] G. Tang and A. Qin, "ECG denoising based on empirical mode decomposition," in *Proc. 9th Int. Conf. Young Computer Scientists*, Hunan, China, 2008, pp. 903−906.

[24] D. Zhang, “Wavelet approach for ECG baseline wander correction and noise reduction,” in *Proc. 27th Annu. Conf. IEEE Engineering in Medicine and Biology Society*, Shanghai, China, 2006, pp. 1212–1215.

[25] M. Kania, M. Fereniec, and R. Maniewski, “Wavelet denoising for multi-lead high resolution ECG signals,” *Meas. Sci. Rev.*, vol. 7, Sec. 2, No. 4, pp. 30−33, 2007.

[26] B. N. Singh and A. K. Tiwari, “Optimal selection of wavelet basis function applied to ECG signal denoising,” *Digit. Signal Process. J.*, vol. 16, pp. 275–287, 2006.

[27] P. M. Agante and J. P. Marques-de-Sá, “ECG noise filtering using wavelets with soft-thresholding methods,” in *Proc. Int. Conf. Computers in Cardiology*, Hannover, Germany, 1999, vol. 26, pp. 535–538.

[28] M. A. Tinati and B. Mozaffary, “A wavelet packets approach to electrocardiograph baseline drift cancellation,” *Int. J. Biomed. Imag.*, pp. 1–9, 2006.

[29] V. Cherkassy and S. Kitts, “Myopotential denoising of ECG signals using wavelet thresholding methods,” *Neural Network*, vol. 14, pp. 1129–1130, 2001.

[30] S. Pooranachandhra, “Wavelet-based denoising using sub-band dependent threshold for ECG signals,” *Digit. Signal Process.*, vol. 18, pp. 49−55, 2008.

[31] P. E. Tikkanen, “Non-linear wavelet and wavelet packet denoising of ECG,” *Biol. Cyber.*, vol. 80, pp. 259−267, 1999.

[32] L.N. Sharma, S. Dandapat, and A. Mahanta, “ECG signal denoising using higher order statistics in wavelet sub-bands,” *Biomed. Signal Process. Control J.*, vol. 5, pp. 214−222, 2010.

[33] P. Mithun, “ECG baseline wander correction and noise reduction,” M.Tech. dissertation, Dept. Biosci. Bioeng., IIT Bombay, Mumbai, India, 2010.

[34] P. Mithun, P. C. Pandey, T. Sebastian, P. Mishra, and V. K. Pandey, “A wavelet based technique for suppression of EMG noise and motion artifact in ambulatory ECG,” in *Proc. 33th Annu. Conf. IEEE Engineering in Medicine and Biology Society*, Boston, Massachusetts, 2011, pp. 7087-7090.

[35] T. Sebastian, “Wavelet based denoising of ECG and ICG signals,” M.Tech. dissertation, Dept. Biosci. Bioeng., IIT Bombay, Mumbai, India, 2011.

[36] L. Si and G. Zhao, “Denoising of ECG signal using translation- invariant wavelet denoising method with improved thresholding,” in *Proc. 27th Annu. Conf. IEEE Engineering in Medicine and Biology Society*, Shanghai, China, 2006, pp. 5946–5949.

[37] S. Li and J. Lin, “The optimal de-noising algorithm for ECG using stationary wavelet transform,” in *Proc. 2009 WRI World Cong. Computer Science Inform. Eng.*, vol. 6, Los Angeles, CA, pp. 469–473.

[38] S. Li, G. Liu, and Z. Lin, “Comparisons of wavelet packet, lifting wavelet and stationary wavelet transform for de-noising ECG,” in *Proc. 2nd IEEE Int. Conf. Computer Science and Information Technology*, Beijing, China, 2009, pp. 491−494.

[39] D. L. Donoho, “De-noising by soft-thresholding,” *IEEE Trans. Inform. Theory*, vol. 41, pp. 613 – 627, 1995.

[40] R. R. Coifman and D. L. Donoho, “Translation invariant de-noising,” in *Wavelets and Statistics*, A. Antoniadis and G. Oppenheim, Eds. New York: Springer-Verlag, 1995, pp. 125–150.

[41] J. Pan and W. J. Tompkins, “A real-time QRS detection algorithm,” *IEEE Trans. Biomed. Eng.*, vol. 32, pp. 230–236, 1985.

[42] P. S. Hamilton and W. J. Tompkins, “Quantitative investigation of QRS detection rules using the MIT/BIH arrhythmia database,” *IEEE Trans. Biomed. Eng.*, vol. 33, pp. 1157–1165, 1986.

[43] PhysioNet, *PhysioBank ATM* [Online]. Available: http://www.physionet.org/cgi-bin/ATM.

[44] PhysioNet, *The MIT-BIH normal sinus rhythm database* [Online]. Available: http://physionet.org/physiobank/database/nsrdb.

[45] PhysioNet, *The MIT-BIH arrhythmia test database* [Online]. Available: http:// www.physionet.org/physiobank/database/mitdb.

[46] PhysioNet, *The MIT-BIH noise stress test database* [Online]. Available: http://www.physionet.org/physiobank/database/nstdb.

[47] PhysioNet, *The MIT-BIH atrial fibrillation database* [Online]. Available: http://www.physionet.org/physiobank/database/afdb.

[48] PhysioNet, *The MIT-BIH ST change database* [Online]. Available: http://physionet.org/physiobank/database/stdb.

[49] PhysioNet, *The MIT-BIH malignant ventricular arrhythmia database* [Online]. Available: http://physionet.org/physiobank/database/vfdb.

[50] PhysioNet, *T-Wave alternans challenge database* [Online]. Available: http://physionet.org/physiobank/database/twadb.

[51] PhysioNet, *Sudden cardiac death holter database* [Online]. Available: http://physionet.org/physiobank/database/sddb.

[52] A. L. Goldberger, L. A. N. Amaral, L. Glass e*t al.* (2000, June 13). “PhysioBank, PhysioToolkit, and PhysioNet: Components of a new research resource for complex physiologic signals,” *Circulation*. [Online]. 101(23), pp. 215-220. Available: http://circ.ahajournals.org/cgi/content/full/101/23/e215.

Acknowledgement

I am grateful to Prof. P. C. Pandey for giving me an opportunity to work under his esteemed guidance for my M. Tech Project. I would like to express my deep gratitude for his valuable suggestions and constant encouragement throughout the project.

I thank P. Mithun and T. Sebastian for their support and critical inputs throughout the project. I would also like to express my sincere thanks to all my lab mates for their help and support during the project work. Last, but not the least, I thank my parents and my family for their support. I dedicate this work to my family and my guide.

T. Pranava

This page is intentionally left blank

Author's Resume

T. Pranava received the B.E. degree in biomedical engineering from SSN College of Engineering, Kalavakkam, Tamil Nadu, affiliated to Anna University, Tamil Nadu in 2010. Presently, she is pursuing the M.Tech. degree in biomedical engineering at the Indian Institute of Technology Bombay. Her current research interests are biomedical signal processing, wavelets, brain-computer interface, and embedded systems.